Article

Structure

Structure of the UHRF1 Tandem Tudor Domain Bound to a Methylated Non-histone Protein, LIG1, Reveals Rules for Binding and Regulation

Graphical Abstract

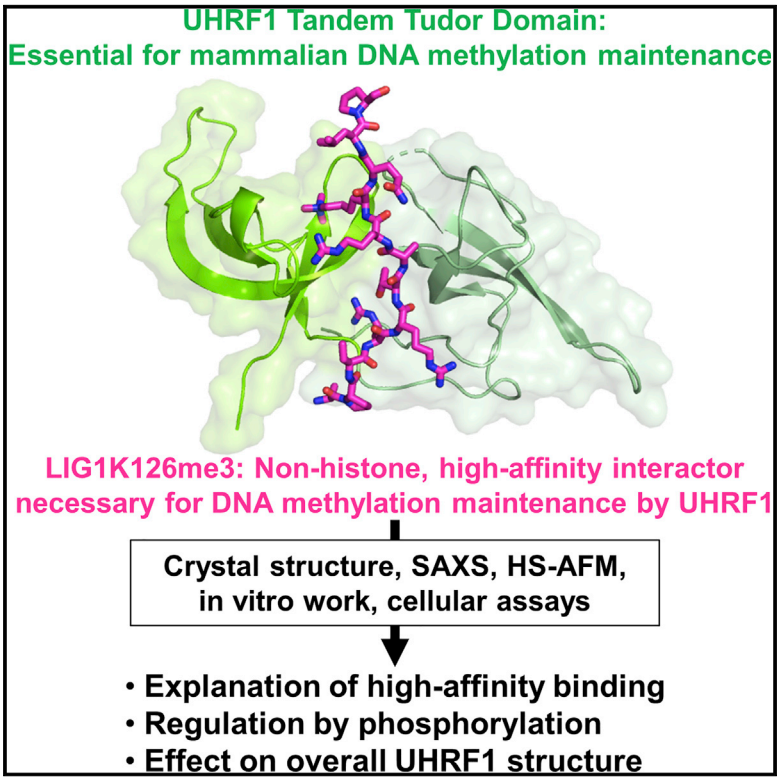

Highlights

- The crystal structure of UHRF1 TTD domain bound to the LIG1K126me3 was determined
- Arg121 of LIG1 is a key residue for high-affinity binding to the TTD
- Phosphorylation of LIG1T123 negatively regulates the interaction with UHRF1
- LIG1K126me3 binding changes UHRF1 structure from closed to open

Authors

Satomi Kori, Laure Ferry, Shohei Matano, ..., Yoichi Shinkai, Pierre-Antoine Defossez, Kyohei Arita

Correspondence

pierre-antoine.defossez@univ-paris-diderot.fr (P.-A.D.), aritak@yokohama-cu.ac.jp (K.A.)

In Brief

The interaction between UHRF1 and LIG1K126me3 is essential for DNA methylation maintenance. Kori et al. determined the crystal structure of the UHRF1 TTD bound to a LIG1K126me3 peptide, revealing the basis for the high TTD-binding affinity of LIG1K126me3, regulation by phosphorylation, and that LIG1K126me3 binding switches the overall structure of UHRF1.

Kori et al., 2019, Structure 27, 485–496
March 5, 2019
https://doi.org/10.1016/j.str.2018.11.012

CellPress

Structure
Article

Structure of the UHRF1 Tandem Tudor Domain Bound to a Methylated Non-histone Protein, LIG1, Reveals Rules for Binding and Regulation

Satomi Kori,[1] Laure Ferry,[2] Shohei Matano,[1] Tomohiro Jimenji,[1] Noriyuki Kodera,[3,4,5] Takeshi Tsusaka,[6] Rumie Matsumura,[1] Takashi Oda,[1] Mamoru Sato,[1] Naoshi Dohmae,[7] Toshio Ando,[3,4] Yoichi Shinkai,[6] Pierre-Antoine Defossez,[2,8,*] and Kyohei Arita[1,5,8,9,*]

[1]Graduate School of Medical Life Science, Yokohama City University, Yokohama 230-0045, Japan
[2]University of Paris Diderot, Sorbonne Paris Cité, Epigenetics and Cell Fate, UMR 7216 CNRS, 75013 Paris, France
[3]Bio-AFM Frontier Research Center, Kanazawa University, Kakuma-machi, Kanazawa 920-1192, Japan
[4]WPI Nano Life Science Institute, Kakuma-machi, Kanazawa 920-1192, Japan
[5]JST, PRESTO, 4-1-8 Honcho, Kawaguchi, Saitama 332-0012, Japan
[6]Cellular Memory Laboratory, RIKEN Cluster for Pioneering Research, Wako, Saitama 351-0198, Japan
[7]Biomolecular Characterization Unit, Technology Platform Division, RIKEN Center for Sustainable Resource Science, Wako, Saitama 351-0198, Japan
[8]Senior author
[9]Lead Contact
*Correspondence: pierre-antoine.defossez@univ-paris-diderot.fr (P.-A.D.), aritak@yokohama-cu.ac.jp (K.A.)
https://doi.org/10.1016/j.str.2018.11.012

SUMMARY

The protein UHRF1 is crucial for DNA methylation maintenance. The tandem Tudor domain (TTD) of UHRF1 binds histone H3K9me2/3 with micromolar affinity, as well as unmethylated linker regions within UHRF1 itself, causing auto-inhibition. Recently, we showed that a methylated histone-like region of DNA ligase 1 (LIG1K126me2/me3) binds the UHRF1 TTD with nanomolar affinity, permitting UHRF1 recruitment to chromatin. Here we report the crystal structure of the UHRF1 TTD bound to a LIG1K126me3 peptide. The data explain the basis for the high TTD-binding affinity of LIG1K126me3 and reveal that the interaction may be regulated by phosphorylation. Binding of LIG1K126me3 switches the overall structure of UHRF1 from a closed to a flexible conformation, suggesting that auto-inhibition is relieved. Our results provide structural insight into how UHRF1 performs its key function in epigenetic maintenance.

INTRODUCTION

Histone modifications and DNA methylation are major epigenetic marks that regulate diverse cellular events by modulating the structure and function of chromatin (Allis and Jenuwein, 2016). In mammals, DNA methylation occurs mostly at the fifth position of cytosine in CpG dinucleotides and plays key roles in development, X chromosome inactivation, genome imprinting, and carcinogenesis (Schübeler, 2015). In proliferating cells, the pattern of DNA methylation has to be re-established after each cycle of DNA replication, and two proteins are known to be key in this process, as their absence causes a similar phenotype of progressive DNA demethylation (Bostick et al., 2007; Sharif et al., 2007; Smets et al., 2017; von Meyenn et al., 2016). The first protein involved is the maintenance DNA methyltransferase, DNMT1, and the other is the protein UHRF1 (ubiquitin-like, containing PHD and RING finger domains, 1).

UHRF1 contains five annotated domains: ubiquitin-like (UBL), tandem Tudor domain (TTD), plant homeodomain (PHD), SET and RING associated (SRA), and RING, and their associated linkers (Figure 1A). The SRA is essential for function and specifically recognizes hemimethylated DNA, which is generated after DNA replication (Arita et al., 2008; Avvakumov et al., 2008; Hashimoto et al., 2008; Liu et al., 2013). Subsequently the RING domain, which has E3 ubiquitin ligase activity, ubiquitylates K14, K18, and/or K23 on histone H3 (hereafter H3), which allows DNMT1 recruitment and activation onto recently replicated sites (Ishiyama et al., 2017; Nishiyama et al., 2013; Qin et al., 2015). The PHD and TTD work cooperatively to recognize the heterochromatin mark H3K9me2/3: the PHD recognizes the N-terminal ^{1}ARTK^{4} motif of the histone, while the TTD accommodates the methylated H3K9me2/3 residue in an aromatic cage (Arita et al., 2012; Cheng et al., 2013; Rajakumara et al., 2011; Rothbart et al., 2013; Zhao et al., 2016). In addition, the TTD also interacts with unmethylated lysine and arginine-rich linkers within UHRF1 itself: the "linker 2" between TTD and PHD finger ($L2_{UHRF1}$) and the "spacer," which follows the SRA domain ($spacer_{UHRF1}$) (Figure 1A) (Arita et al., 2012; Cheng et al., 2013; Fang et al., 2016; Gao et al., 2018; Gelato et al., 2014). These intramolecular interactions lead to a "closed" overall structure of UHRF1 and the auto-inhibition of DNA binding and E3 activities (Fang et al., 2016; Gelato et al., 2014; Harrison et al., 2016).

We recently showed that the TTD of UHRF1 interacts with a histone-like sequence within a replication protein, DNA ligase 1 (LIG1) (Ferry et al., 2017). Molecularly, LIG1 contains an intrinsically disordered region at its N-terminus (residues 1–200), within which residues 118–130 are similar to the H3 N-terminal tail

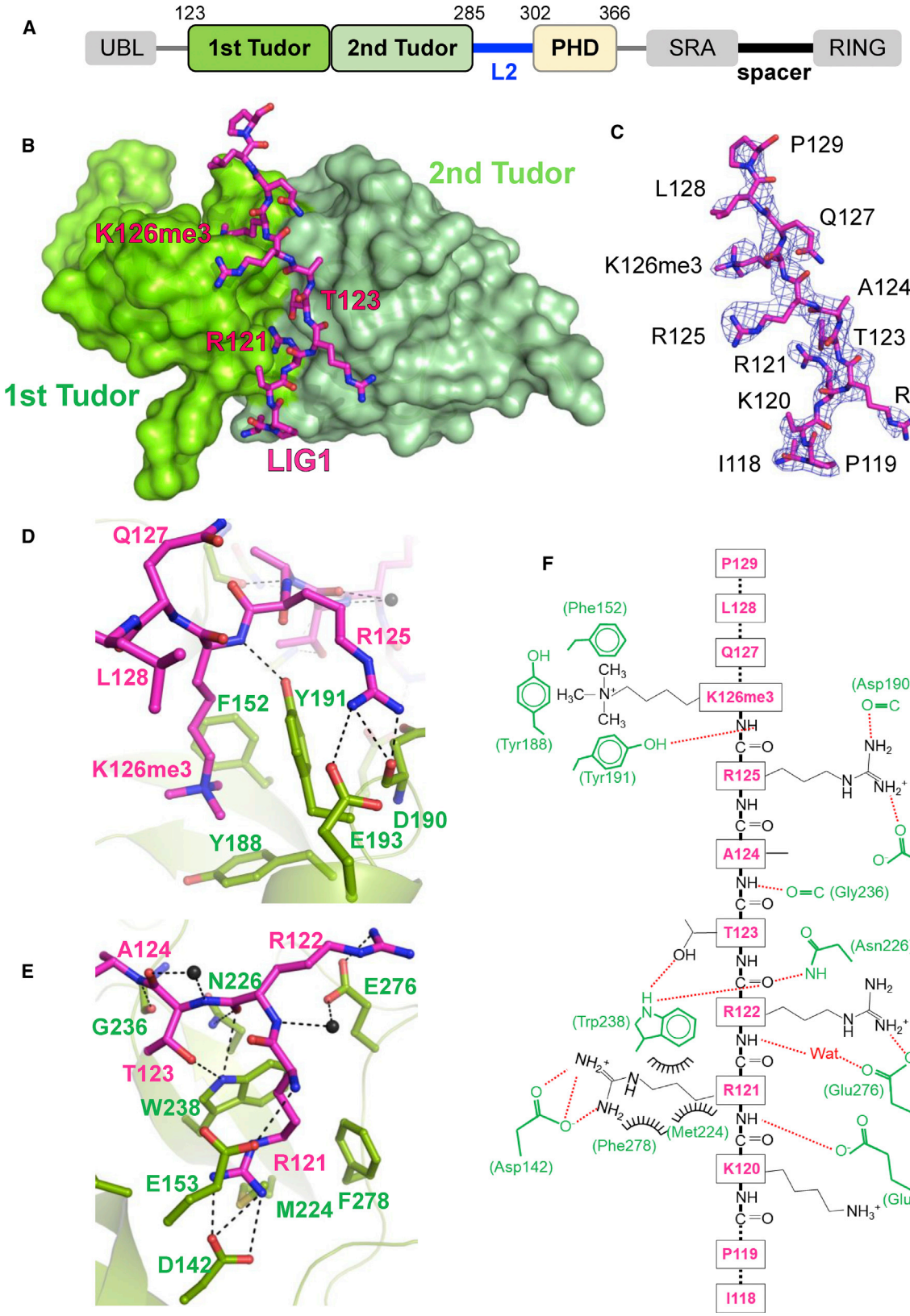

(legend on next page)

Table 1. Data Collection and Refinement Statistics

	apo-TTD (PDB: 5YYA)	TTD:LIG1K126me3 (PDB: 5YY9)
Data Collection		
Space group	$P2_12_12_1$	$P2_12_12_1$
Cell dimensions		
a, *b*, *c* (Å)	38.8, 60.0, 68.9	27.1, 97.3, 132.5
Resolution (Å)	45.25–1.70 (1.73–1.70)[a]	48.67–2.65 (2.78–2.65)[a]
R_{sym} or R_{merge} (%)	4.3 (22.6)[a]	12.2 (70.2)[a]
$I/\sigma(I)$	25.1 (5.3)[a]	8.5 (2.4)[a]
$CC_{1/2}$	99.9 (92.8)[a]	99.2 (89.1)[a]
Completeness (%)	97.9 (80.2)[a]	97.0 (95.4)[a]
Redundancy	6.5 (3.9)[a]	3.8 (3.8)[a]
Total reflections	117,437	40,019
Unique reflections	17,949	10,403
Refinement		
Resolution (Å)	34.35–1.70 (1.81–1.70)[a]	40.23–2.65 (2.79–2.65)[a]
No. of reflections	17,884 (1517)[a]	10,368 (989)[a]
R_{work}/R_{free} (%)	17.2/20.6	23.1/28.8
No. atoms		
Protein	1,335	2,379
Ion	1	0
Water	244	24
B factors		
Protein	21.19	44.41
Ion	27.75	–
Water	33.11	37.91
RMSD		
Bond lengths (Å)	0.004	0.005
Bond angles (°)	0.63	0.84

[a]Values in parentheses are for the highest-resolution shell.

(residues 1–12), and LIG1K126 is in a sequence environment similar to H3K9. Furthermore, LIG1K126 is methylated by the lysine methyltransferases G9a (EHTM2) and GLP (EHTM1) *in vitro* and in cells. We found that a LIG1K126me3 peptide largely outcompetes H3K9me2/3 peptides for binding to the UHRF1 TTD. We also reported that the aromatic cage of the TTD was necessary for binding, yet a number of molecular questions remain open as to how UHRF1 interacts with this methylated non-histone protein. What are the similarities between H3K9me2/3 and LIG1K126me3 binding? What are the differences, and how do they contribute to the higher affinity binding to LIG1? What is the effect of LIG1 binding to the overall UHRF1 architecture and function?

To address these questions, we have solved the crystal structure of the UHRF1 TTD in complex with a methylated LIG1 peptide. The structure, complemented by mutagenesis and functional assays reveals key residues for the interaction, sheds light on the mechanism for high-affinity binding of LIG1 to TTD, and indicates that the binding event causes a large-scale molecular reorganization within UHRF1. Our data provide insight into UHRF1 binding to a methylated non-histone protein, and contribute to understanding its key role in epigenetic maintenance.

RESULTS

The TTD in Complex with LIG1K126me3 Peptide Adopts a Canonical Structure

We first produced and crystallized the wild-type (WT) human TTD (residues 123–285); a structure was obtained at 1.7 Å resolution (apo-TTD, Figure S1A; Table 1). The co-crystallization of this WT construct with the LIG1K126me3 peptide was, however, unsuccessful. Based on the structure of the unliganded TTD (Figure S1A), we speculated that a flexible loop might be interfering with co-crystallization, so we generated and tested mutant versions of the TTD lacking this loop. After optimization trials, for co-crystallization we used a variant TTD (vTTD from here on) in which the loop is removed by deleting residues 167–175. The vTTD has the same binding affinity for LIG1K126me3 as the WT TTD, as measured by isothermal titration calorimetry (ITC) (Figure S1B). The LIG1 peptide contained residues 118–130 of the human protein, with the key lysine K126 trimethylated (K126me3).

We determined the crystal structure of vTTD with LIG1K126me3 peptide at 2.65 Å resolution (Table 1); in the crystal, an asymmetric unit contained two vTTD:LIG1K126me3 complexes. The structures of the two vTTDs in the unit were identical (root-mean-square deviation [RMSD] of Cα atoms 1.4 Å over the 125 Cα atoms) (Figure S1A). The structure of LIG1K126me3 peptides in the asymmetric unit was also identical (RMSD of Cα atoms 0.5 Å) (Figure S1C). The 12 successive residues from Ile118 to Pro129 showed clear electron density in the $|F_o| - |F_c|$ omit map (Figures 1B and 1C), and are described hereafter.

The overall TTD structure was virtually identical with or without the LIG1K126me3 peptide (RMSD of Cα atoms 0.8–1.6 Å) (Figure S1A), implying that binding of the LIG1K126me3 did not lead to the structural rearrangement of the TTD. As in previously published structures (Fang et al., 2016; Nady et al., 2011), the first and second Tudor domains comprised a five-stranded β barrel fold, and the two domains were separated by a groove

Figure 1. Structure of the UHRF1 TTD in Complex with a LIG1K126me3 Peptide

(A) Schematic of the domain organization of UHRF1. The amino acid numbers in the human protein are indicated.

(B) Overall structure of TTD:LIG1K126me3 complex. The first and second Tudor domains are shown as yellow-green and pale-green surface models, respectively. LIG1 is depicted as a magenta stick model.

(C) The LIG1 peptide and $|F_o| - |F_c|$ omit map contoured at 2 σ are colored magenta and blue, respectively.

(D and E) Recognition of R125-K126me3 (D) and R121-A124 (E) of LIG1 by the TTD. Color schemes are the same as in (B). Water molecules are represented as black balls.

(F) Schematic diagram of LIG1K126me3 recognition by the TTD. The LIG1 backbone and side chains are shown in black and TTD residues in green. Dotted lines and black arcs with spokes indicate hydrogen bonds and hydrophobic interactions, respectively.

Supplemental data are provided in Figure S1.

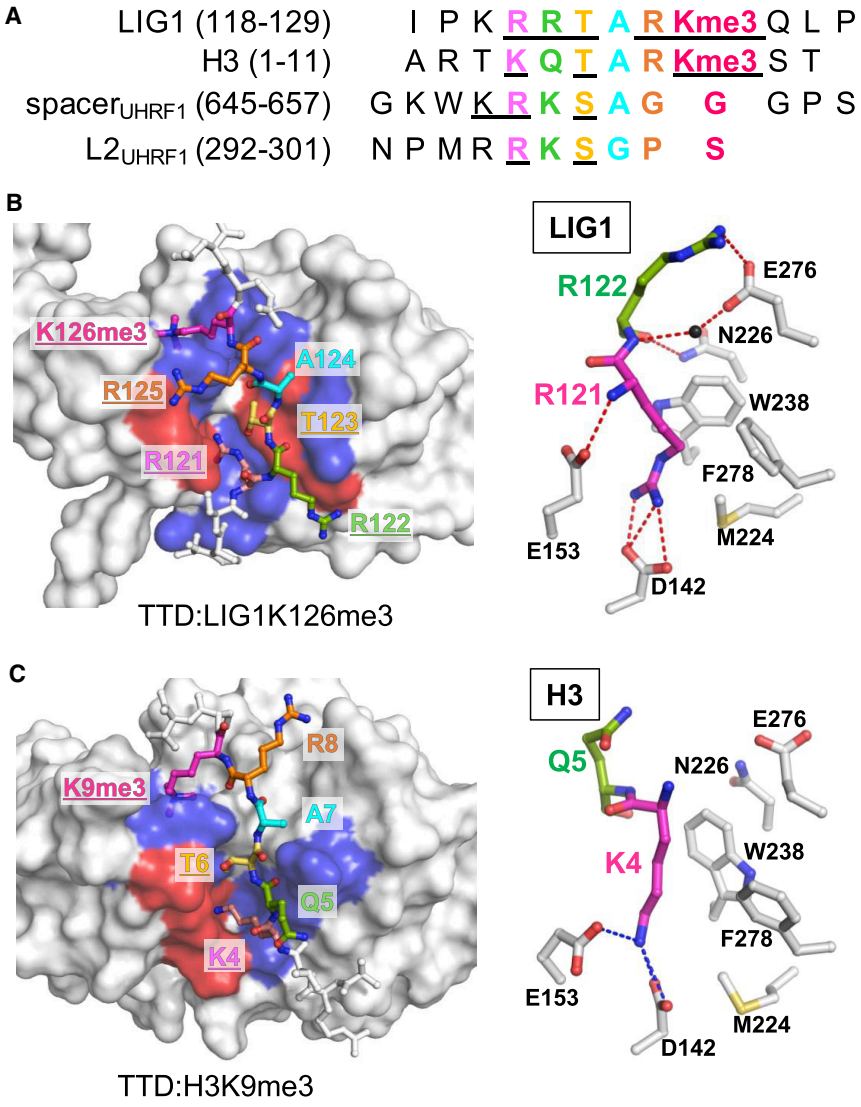

Figure 2. Structural Comparison of TTD Binding Partners

(A) Sequence alignment of LIG1, H3, spacer$_{UHRF1}$, and L2$_{UHRF1}$. The residues underlined have a side chain that interacts with the TTD.

(B and C) Structure around the TTD groove in complex with LIG1K126me3 (B) and H3K9me3 (C) (PDB: 2L3R). Each peptide is shown as a stick model and the color schemes are same in (A). Red and blue on the surface of TTD indicate hydrophilic and hydrophobic interaction residues, respectively. Right panel is the structure around Arg-binding cavity in TTD complexed with LIG1K126me3 (B) and H3K9me3 (C). Color scheme of LIG1 and H3 are same as in (A) and TTD residues are shown as gray stick model.

Supplemental data are provided in Figure S2.

(TTD groove from here on, Figures 1B and S1A). The LIG1K126me3 peptide interacted in an extended conformation with the TTD groove and, within the peptide, residues Arg121 to Lys126me3 contacted TTD residues (Figures 1B–1F).

Two Regions of the LIG1K126me3 Peptide Establish Dense Contacts with the TTD

The structure showed that two clusters of dense contacts between TTD and LIG1 peptide participated in the stable complex formation. First, the aromatic cage comprising Phe152, Tyr188, and Tyr191 of UHRF1 interacted with the tri-methyl moiety of K126me3 in LIG1 (Figures 1D and 1F). Second, the side chain of LIG1Arg121 was inserted into a depression of the TTD groove, designated as an "Arg-binding cavity"; there, the guanidino group and aliphatic portion of Arg121 were recognized by multiple hydrogen bonds and hydrophobic interactions with side chains of UHRF1-Asp142 and Met224, Trp238, and Phe278, respectively (Figures 1E and 1F). Of these positions, Asp142, Met224, and Trp238 are almost invariant within UHRF1 orthologs found in animal species, whereas Phe278 is less strictly conserved (Figure S2A). In addition to these dense contacts, the side chains of Arg122 and Arg125 of LIG1 were recognized by the side chain of Glu276 and the main chain of Asp190 of TTD, respectively (Figures 1D–1F). Glu193 of TTD also supported the binding to LIG1Arg125 by long-range electrostatic interaction (~3.7 Å) (Figure 1D). The side chain of LIG1Thr123 formed additional hydrogen bonds with the side chain of UHRF1-Trp238 (Figures 1E and 1F). Finally, the main chains of Arg121, Arg122, Ala124, and K126me3 in LIG1 were also involved in the interaction with TTD (Figures 1D–1F).

LIG1R121 Plays a Key Role for the High-Affinity Interaction between TTD and LIG1K126me3

Our published work (Ferry et al., 2017), as well as data presented here, suggest that the TTD of UHRF1 has much higher affinity for methylated LIG1 than for its other reported interactors: H3K9me3, spacer$_{UHRF1}$, and L2$_{UHRF1}$ (Arita et al., 2012; Fang et al., 2016; Gelato et al., 2014; Nady et al., 2011). To understand the basis for this preference, we compared the peptide sequences and structural data for these interactions (Figures 2A–2C). Of all the interacting peptides, H3 has the clearest sequence similarity to LIG1 (KQTARK versus RRTARK, see Figure 2A); it also has a similar binding mechanism, interacting both with the aromatic cage and Arg-binding cavity of the TTD (Figures 2B and 2C). However, the binding affinity of LIG1K126me3 for the TTD, determined by ITC, was approximately 180 times higher than that of H3K9me3 (K_D = 1,620 nM for H3K9me3 versus K_D = 9.1 nM for LIG1K126me3, Table 2, and ITC thermograms in Figures S1B and S2B). The major sequence differences between peptides are Lys4 and Gln5 of H3, which are in the position of Arg121 and Arg122 of LIG1, respectively, so we mutagenized these positions within an H3K9me3 peptide and determined the consequences for TTD binding (Table 2; Figure S2B). Replacing H3K4 by Arg dramatically increased the binding affinity for TTD

Table 2. Summary of ITC Measurements

TTD	LIG1 or H3	K_D (nM)
WT	LIG1K126me3	9.1 ± 3.8
WT	LIG1K126me0	250 ± 35
	LIG1T123ph/K126me3	>104,500
	LIG1R121A/K126me3	>55,000
	LIG1R125A/K126me3	21.4 ± 1.1
D142A	LIG1K126me3	ND
Y188A/Y191A		5,537 ± 490
E193A		23.0 ± 8.2
E276A		49.7 ± 11
W238A		1,056 ± 35
WT	H3K9me3	1,620 ± 111
	H3K4R/K9me3	22.2 ± 4.4
	H3Q5R/K9me3	1,440 ± 17
	H3K4R/Q5R/K9me3	13.8 ± 0.8

ND, not determined.

(K_D = 22.2 nM, similar to that of LIG1K126me3, K_D = 9.1 nM); in contrast, replacing H3Q5 by Arg had no effect on the binding affinity (K_D = 1,440 nM). The double-substituted peptide H3K4R/Q5R behaved like the single K4R-substituted peptide (K_D = 13.8 nM).

These experiments show that the presence of an arginine residue at position 121 of LIG1 (in contrast to the lysine residue found at the equivalent H3 position 4) is a key contributor to the high-affinity binding. This can be explained by comparing our structure to the previously published TTD:H3K9me3 structure (Figures 2B and 2C). Indeed, the side-chain conformations of Arg121 in LIG1K126me3 and Lys4 in H3K9me3 markedly differ: Arg121 establishes hydrogen bonds with TTD-Asp142 via its guanidine group, and CH-π interactions with TTD-Trp238 and TTD-Phe278 via its alkyl group, all of which likely contribute to the high-affinity interaction (Figure 2B). The difference in side-chain length between lysine and arginine also affects the main-chain conformation, allowing a higher number of interactions for LIG1, as the side chains of residues Arg122 and Arg125 form with the TTD contacts not formed by H3 (Figures 2A and 2B).

Mutational Analysis Validates the Structural Data and Uncovers a Phospho-Switch Regulation

To validate our structural data and quantify the contribution of individual residues to the interaction, we performed ITC experiments using WT or mutated versions of the TTD and LIG1 peptide (Table 2; Figure S3A). The values obtained with WT partners were consistent with our previous report (Ferry et al., 2017): the TTD bound LIG1K126me3 with a K_D = 9.1 nM, and LIG1K126me0 with a K_D = 250 nM (Table 2; Figures S1B and S3A).

We tested several mutations of the TTD: the mutation with the most deleterious effect was D142A, which obliterated any detectable binding. The second most deleterious change was inactivation of the aromatic cage, using the double mutation Y188A/Y191A; this resulted in detectable binding but vastly reduced affinity for LIG1K126me3 (K_D = 5,537 nM). Mutation W238A also had a large effect, reducing the affinity by 100-fold (K_D = 1,056 nM). Finally, mutations E193A and E276A had smaller but measurable effects on the UHRF1/LIG1K126me3 interaction. These results are consistent with our structural data.

Next, we introduced mutations in the LIG1K126me3 peptide. The R121A change had a severe effect, reducing binding by at least 6,000-fold (K_D > 55,000 nM); in contrast, the R125A mutation only led to a slight binding reduction (K_D = 21.4 nM). Finally, it has been observed that phosphorylation of Thr6 of H3, Ser298 of $L2_{UHRF1}$, and Ser651 of $spacer_{UHRF1}$ inhibits the interaction with the TTD (Arita et al., 2012; Fang et al., 2016; Gelato et al., 2014; Rothbart et al., 2013), so we tested whether a similar effect might also occur when LIG1 is phosphorylated on the equivalent residue, Thr123. We synthetized a peptide in which LIG1K126 was trimethylated, LIG1T123 phosphorylated; this peptide interacted extremely poorly with the TTD (K_D > 104,500 nM), establishing that phosphorylation at Thr123 is indeed inhibitory to the interaction.

We next sought to identify a kinase that could phosphorylate LIG1T123. The equivalent position in H3, H3T6, is phosphorylated by protein kinase Cβ (PKCβ) (Metzger et al., 2010), so we tested whether PKCβ also phosphorylates LIG1T123. *In vitro* phosphorylation assay combined with mass spectrometry demonstrated that LIG1T123 was indeed efficiently phosphorylated by the kinase, independent of the Lys126 methylation status (Figure 3A), suggesting that PKCβ is a candidate for LIG1T123 phosphorylation in the cell.

Validation of the Structural Data by a Cellular Assay Reveals the Importance of LIG1R125 for Methylation of LIG1K126

We also examined the interaction by an independent technique, the fluorescent three-hybrid assay (F3H) (Herce et al., 2013). In this approach, proteins bearing fluorescent tags are co-expressed in an engineered mammalian cell line, which is designed so that the GFP-tagged protein will be recruited to a nuclear spot. The percentage of cells in which the RFP-tagged protein forms a spot co-localizing with the GFP spot is then recorded, and provides a direct estimate of the interaction propensity in cells (schematic in Figure 3B). We carried out this assay with full-length UHRF1 fused to GFP, and full-length LIG1 fused to dsRed, using WT proteins or introducing the mutations studied by ITC. The F3H results agreed very well with ITC: mutation D142A in UHRF1 had a severe effect, W238A was less marked, and E193A and/or E276A had smaller effects (Figures 3C and S3B). Within LIG1, the R121A mutation totally abrogated interaction, and so did the phosphomimetic T123D mutation. A striking difference with the ITC results is that the LIG1R125A mutation, which had little effect in ITC, led to total loss of interaction in the F3H assay (Figures 3C and S3B). G9a and GLP favor an RK motif in their targets to efficiently catalyze lysine methylation (Rathert et al., 2008), so we postulated that the LIG1R125A mutation could affect the interaction with the TTD indirectly, by decreasing LIG1K126 methylation.

We tested this hypothesis *in vitro* by incubating LIG1 peptides with recombinant G9a, and then detecting lysine methylation by MALDI-TOF (Figure 3D). As described previously (Ferry et al., 2017), G9a efficiently trimethylated the LIG1 peptide. The LIG1R121A mutation had very little effect on methylation by G9a. In contrast, the LIG1R125A mutation had a major effect,

A

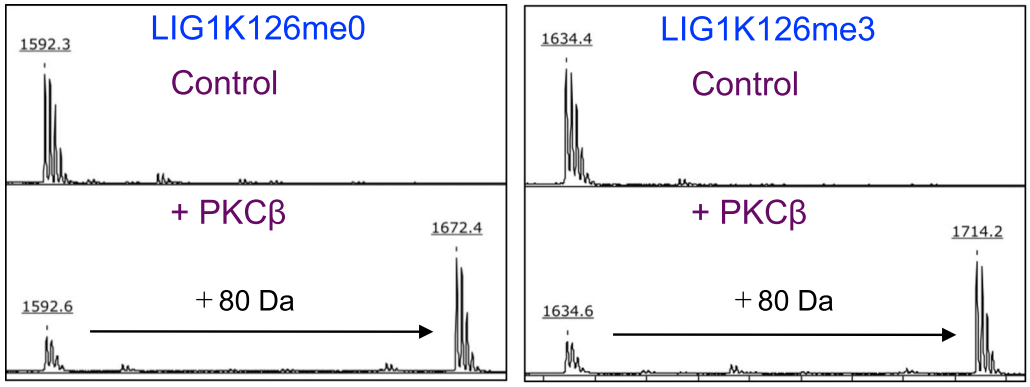

B

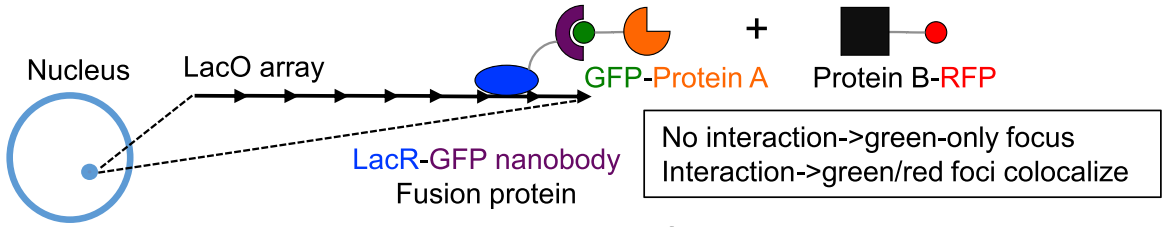

C

Plasmid cotransfected with DsRed-LIG1: GFP-UHRF1 with following mutations				
WT	D142A	E193A	E276A	W238 A
90%	1%	84%	55%	38%
% cells with green/red colocalization				

Plasmid cotransfected with GFP-UHRF1: DsRed-LIG1 with following mutations			
WT	R121A	T123D	R125A
90%	0%	0%	0%
% cells with green/red colocalization			

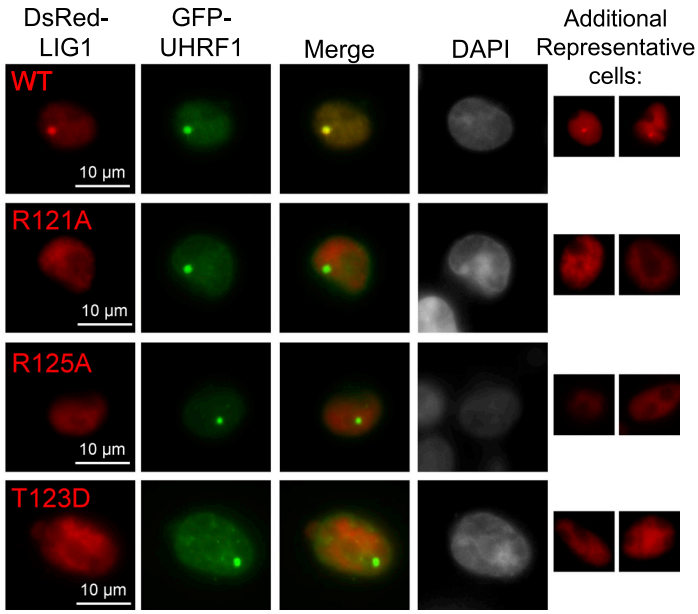

D

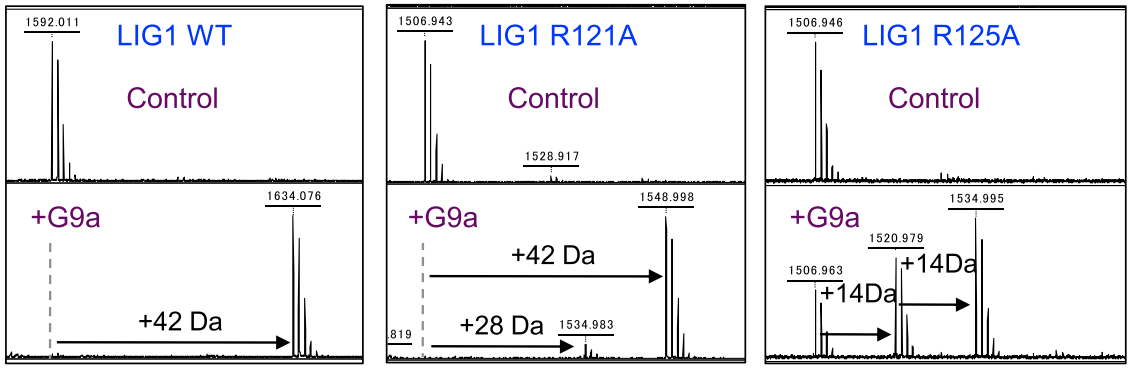

(legend on next page)

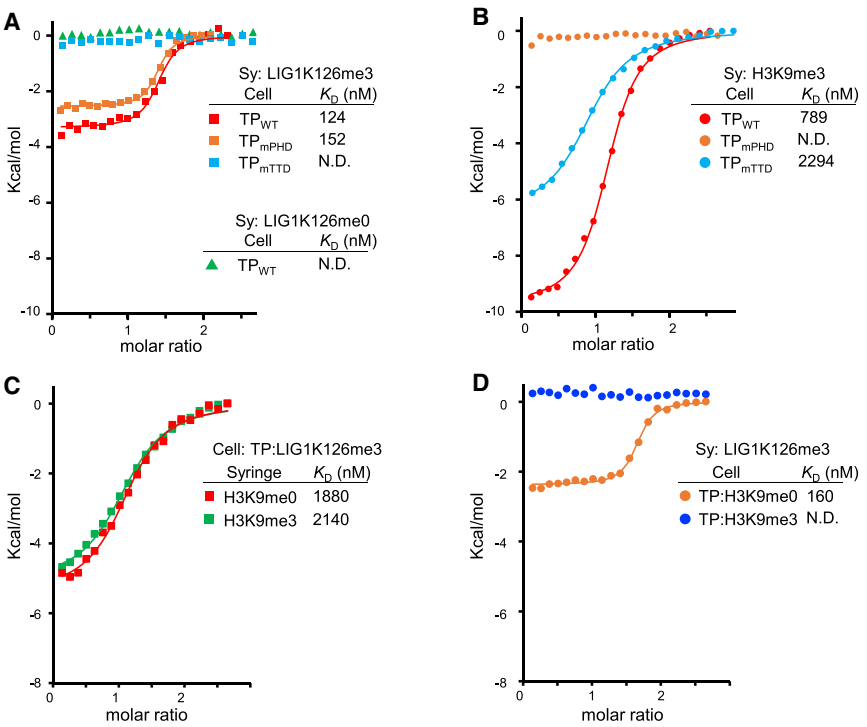

Figure 4. Stepwise Binding of LIG1K126me3 to the TTD-PHD Module

(A) Superimposition of enthalpy change plots for (A) binding of LIG1K126me3 peptide to TTD-PHD (abbreviated TP) with the indicated mutations and LIG1K126me0 to WT TP. The binding affinities and samples in the syringe (Sy) and cell are indicated.

(B) Binding of H3K9me3 peptide to TP with the indicated mutations.

(C) Binding of H3K9me0 or H3K9me3 peptides to TTD-PHD in the presence of LIG1K126me3.

(D) Binding of LIG1K126me3 to TTD-PHD in the presence of H3K9me0 or H3K9me3.

Supplemental data are provided in Figure S4.

totally preventing trimethylation by G9a (Figure 3D). Similar results were obtained with GLP (not shown). These *in vitro* data strongly suggest that reduced methylation of LIG1K126 is the reason why the LIG1R125A mutant fails to interact with the UHRF1 TTD in a cellular assay. Altogether, the data from ITC and F3H are fully consistent with the structure we obtained: they show that the ionic interaction between Asp142 of TTD and Arg121 of LIG1 plays a foremost role in the binding, followed by the hydrophobic interaction between LIG1K126me3 and the TTD hydrophobic cage. Lastly, we have shown that the interaction can be negatively regulated by phosphorylation of LIG1T123.

LIG1K126me3 Binds to TTD-PHD in a Way Distinct from H3

The adjacent TTD and PHD domains of UHRF1 form a functional unit for binding H3K9me3, in which $L2_{UHRF1}$ interacts with the TTD groove, the N-terminus of H3 binds the PHD, and the H3K9me3 residue inserts into the aromatic cage of the TTD (Arita et al., 2012; Fang et al., 2016; Gelato et al., 2014). We next asked whether LIG1 binding obeyed similar rules, by performing binding assays with WT or variant TTD-PHD (TP) units. The LIG1K126me3 peptide bound to the WT TP with a K_D = 124 nM, whereas the LIG1K126me0 peptide did not show any detectable binding (Figures 4A, S4A, and S4B). As we previously found that the LIG1K126me0 peptide binds the isolated TTD with a K_D = 250 nM (our previous work [Ferry et al., 2017] and Table 2), we conclude that its binding to TP is prevented, presumably by $L2_{UHRF1}$ occupying the TTD groove.

To discern the relative contributions of TTD and PHD to the binding, we used two mutant forms of the TP: the Y188A/Y191A mutant that has an inactivated TTD aromatic cage (hereafter TP_{mTTD}), and the D334A/D337A mutant that loses the PHD function (TP_{mPHD}). When incubated with LIG1K126me3, the TP_{mTTD} showed no detectable binding, while TP_{mPHD} behaved like the WT form (Figures 4A and S4A). Conversely, when incubated with H3K9me3, TP_{mTTD} bound the peptide, but TP_{mPHD} did not (Figures 4B and S4C), consistent with the published finding that H3K9me3 must engage the PHD to bind TP (Cheng et al., 2013). These results imply that binding of LIG1 to the TP is strictly dependent on K126 methylation and is limited to the TTD moiety. In support of this hypothesis, we found that LIG1K126me3 could not bind the isolated PHD (Figure S4D). This might be explained by the fact that LIG1 has no basic residue equivalent to H3R2, a critical contributor to PHD binding by H3 (Figure 2A).

Next, we examined whether H3K9me3 and LIG1K126me3 could simultaneously bind to TP; for this, we pre-complexed the TP with peptides of interest, and measured binding to the other peptides (Figures 4C, 4D, S4E, and S4F). H3K9me0 and H3K9me3 peptides could bind to the TP pre-complexed with LIG1K126me3 with a K_D of 1,880 and 2,141 nM, respectively. These affinities are comparable with that of the isolated PHD for the N-terminus of H3 (Arita et al., 2012), suggesting that LIG1K126me3 bound to the TTD moiety does not prevent N-terminus of H3 binding the PHD moiety (Figures 4C and S4E). Pre-complexing the TP with H3K9me0 did not decrease its affinity for LIG1K126me3 with a K_D of 159 nM, while pre-complexing with H3K9me3 totally abolished binding (Figures 4D and S4F).

Figure 3. Mutation Analysis Confirms the Structural Data and Uncovers a Negative Regulation by Phosphorylation

(A) *In vitro* phosphorylation assay of $LIG1_{118-130}$ peptides by PKCβ. The mass shift of +80 Da detected by MALDI-TOF mass analysis, indicates phosphorylation.

(B) Principle of the F3H assay.

(C) Results of the F3H assay: mutations in the UHRF1 TTD affect interaction with LIG1 and mutations in LIG1 affect interaction with the UHRF1 TTD. The scale bar represents 10 μm.

(D) *In vitro* methylation assay of $LIG1_{118-130}$ peptides by G9a. Each methylation event adds 14 Da to the peptides. The R125A mutation inhibits methylation by G9a.

Supplemental data are provided in Figure S3.

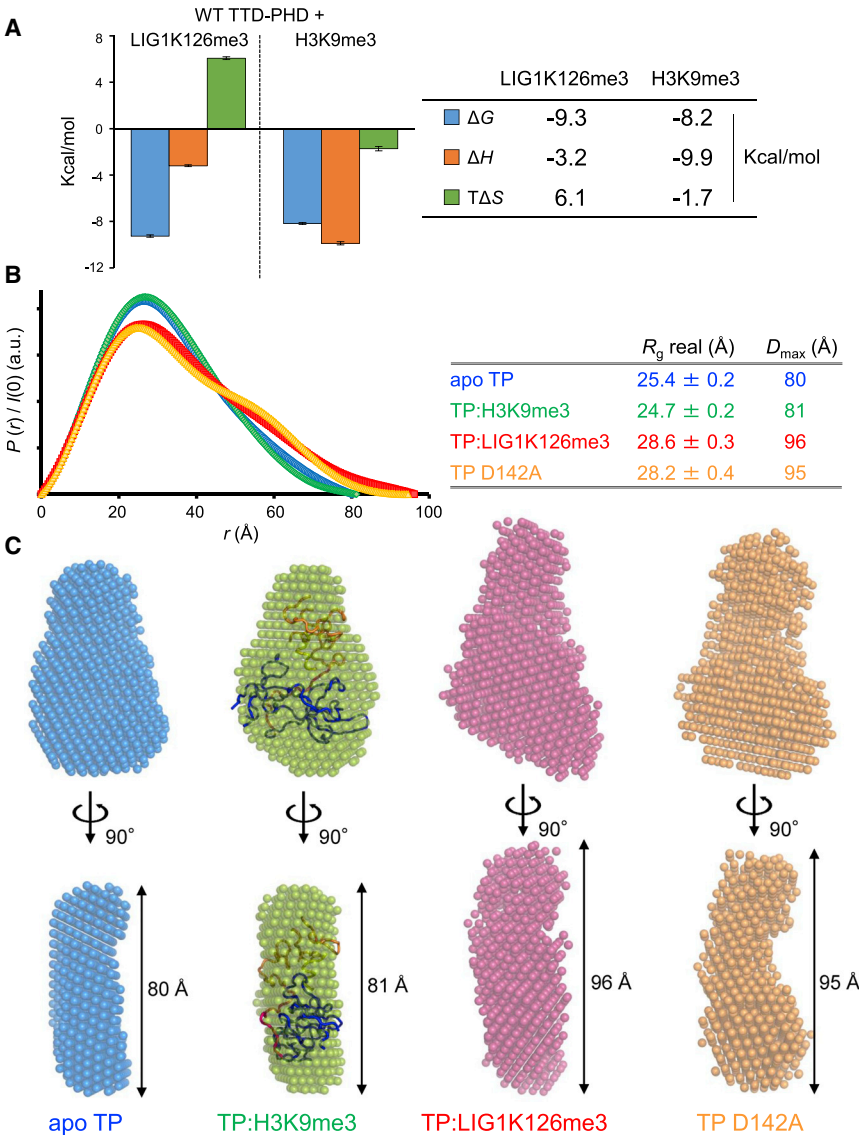

Figure 5. LIG1 Binding Decreases the Compactness of TTD-PHD

(A) Thermodynamic data of binding of LIG1K126me3 and H3K9me3 peptide to the TTD-PHD determined by ITC. Data are represented as mean ± SD.

(B) SAXS experiments on the TTD-PHD module (TP). *P*(*r*) functions are shown for apo-TP (blue) its complex with H3K9me3 (green) and LIG1K126me3 peptides (red) and TP harboring D142A mutant (orange). R_g and D_{max} values are also shown.

(C) Low-resolution *ab initio* models derived from SAXS data.

Supplemental data are provided in Figures S5–S8.

A possible interpretation of the results is that the binding of H3K9me3 stabilizes the TTD-PHD in a "locked" conformation in which $L2_{UHRF1}$ occupies the TTD groove, preventing access of LIG1K126me3. Alternatively, the data could indicate that a free TTD aromatic cage is crucial for the binding of LIG1 to UHRF1. This would suggest a two-step model of LIG1K126me3 binding to the TP, the first step being access of LIG1K126me3 to the aromatic cage of the TTD, and the second being LIG1R121 inserting into the Arg-binding cavity of the TTD groove.

Binding to LIG1 Changes the Arrangement of the TTD-PHD Module and the Overall UHRF1 Structure

Next, we calculated the different thermodynamic parameters of LIG1K126me3 and H3K9me3 binding to the TP from ITC experiments, as these can give insight into the nature of the binding mode (Du et al., 2016). We found that these parameters were markedly different: the binding of H3K9me3 was enthalpy driven, with a ΔH of large negative value (−9.9 kcal/mol, Figure 5A), while the binding of LIG1K126me3 was entropy-driven, with a positive $T\Delta S$ value (6.1 kcal/mol, Figure 5A). The enthalpy-driven binding of H3K9me3 is consistent with its known mode of interaction, in which the binding occurs without conformational change of TP (Arita et al., 2012). The entropy-driven binding of LIG1K126me3, in contrast, is suggestive of a rearrangement of the TP, and a likely candidate for this is a displacement of $L2_{UHRF1}$ from the TTD groove.

To verify that a structural change in the TP does take place upon binding of LIG1K126me3, we used size-exclusion chromatography in line with small-angle X-ray scattering (SEC-SAXS) (Figures 5B, S5, and S6; Table S1). Purified TP, in its unliganded apo form, or in complex with H3K9me3 or LIG1K126me3 peptide, was loaded on the SEC and the eluted fractions were exposed by X-ray beam. We also included a mutant TP with the D142A, which prevents interaction between the TTD groove and the $L2_{UHRF1}$, thereby opening the structure (Fang et al., 2016; Gelato et al., 2014; Harrison et al., 2016).

The molecular mass of the samples estimated by comparing $I(0)/c$ (where c is the protein concentration) of the standard sample (bovine carbonic anhydrase) established that there was no aggregation of the measured samples (Figure S5). The radius of gyration (R_g), the distance distribution function $P(r)$, and the maximum dimension of particles (D_{max}) for each scattering image at the peak of absorption at 280 nm (A_{280}), and the $I(0)$ of the each sample were calculated (Figures 5B and S6). The numbers obtained for unliganded TP were similar to those previously reported (Arita et al., 2012; Houliston et al., 2017), and they were not affected by the addition of H3K9me3 peptide, consistent with an absence of overall structural rearrangement (Figures 5B, S5A, S5B, S6A, and S6B). In contrast, the addition of LIG1K126me3 caused a marked increase in the R_g and D_{max} values, implying a rearrangement of the TTD-PHD module to a more extended form. The structural change was very similar to that seen upon the D142A

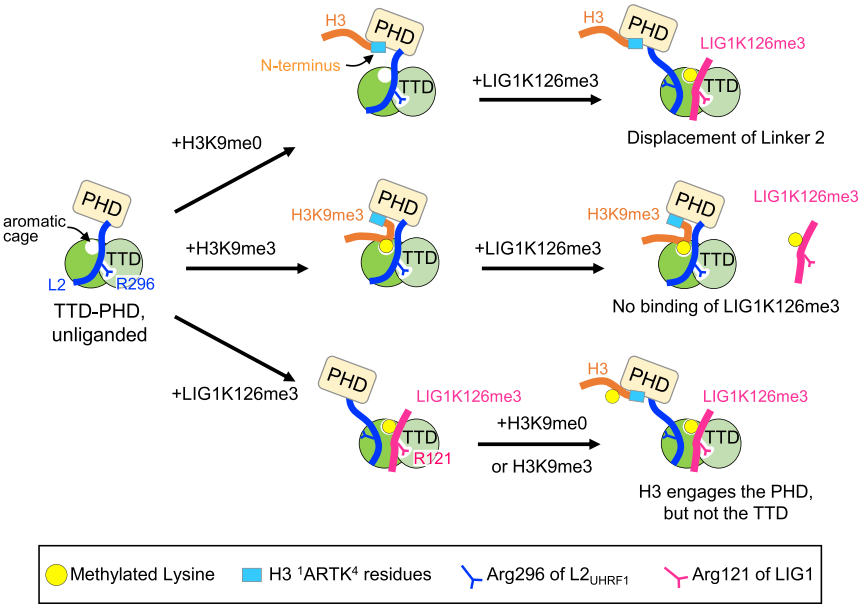

Figure 6. Schematic Model for the Different Binding Characteristics of LIG1 and H3 to UHRF1 TTD-PHD

Summary and interpretation of the data. The yellow sphere and cyan box represent methylated lysine and H3 N-terminal ^{1}ARTK^{4} residues, respectively.

mutation (Figures 5B, S5C, S5D, S6C, and S6D). An *ab initio* shape reconstruction from scattering data yielded highly similar shapes for unliganded TP and TP bound to H3K9me3 (Figure 5C). In contrast, the shape of TP bound to LIG1K126me3 was more extended, and similar to that of TP D142A mutant (Figure 5C). This is compatible with the possibility that LIG1K126me3 binding displaced $L2_{UHRF1}$ from the groove (Figure 6).

We also examined the overall structure of full-length UHRF1. As full-length UHRF1 tends to aggregate (our unpublished data), it was not amenable to SEC-SAXS, but we could employ an independent approach, high-speed atomic force microscopy (HS-AFM). We found that unliganded full-length UHRF1 appeared as a compact molecule, whereas it became more extended and its conformational flexibility increased upon binding of LIG1K126me3 (Figures S7 and S8; Videos S1, S2, and S3).

These data show that LIG1 binding alters the overall structure and dynamics of the TTD-PHD module but also of full-length UHRF1.

DISCUSSION

We report the structure of the UHRF1 TTD bound to a methylated non-histone protein, LIG1. The UHRF1/LIG1 interaction is physiologically important, as it permits the recruitment of UHRF1 to replicating DNA, and the maintenance of DNA methylation, an essential epigenetic mark in mammals (Ferry et al., 2017). Our structural data are validated by independent biochemical and cellular approaches, and they shed light on three important questions: what distinguishes LIG1 interaction from interaction with other UHRF1 TTD binders? What mechanisms may modulate the LIG1/UHRF1 interaction? Finally, how does this interaction affect the overall structure of UHRF1?

Structure of the UHRF1 TTD Complexed with LIG1 Reveals Commonalities and Differences with Other Interactors

The TTD of UHRF1 binds histone and non-histone proteins. This property has already been described for a few other cases, and one well-characterized example is 53BP1: its TTD can bind H4K20me2 (Botuyan et al., 2006), but also RbK810me2 (Carr et al., 2014) and p53K370me2 (Tong et al., 2015). We present an example of a TTD binding a non-histone protein with an affinity far greater than its affinity for histones, and moreover we can explain this binding behavior structurally.

A first conclusion from our data is that the TTD engages LIG1 in a manner similar to its other targets: the LIG1 peptide was extended in the TTD groove as previously reported for H3, the $L2_{UHRF1}$, and $spacer_{UHRF1}$. Another commonality between the various interactions is that they all involve a basic residue (Arg or Lys, R121 in the case of LIG1) in the binder, which penetrates deep into the Arg-binding cavity of the groove and forms an electrostatic interaction with Asp142 of UHRF1, a residue highly conserved through evolution. It is noteworthy that Arg121 is in position equivalent to H3K4, and that lack of methylation at H3K4me0 is a prerequisite for DNA methylation to occur. Finally, another similarity with previous structures is that the methylated lysine (LIG1K126me3) is accommodated by the aromatic cage formed of UHRF1 Phe152, Tyr188, and Tyr191, as is the case for H3K9me3 (Arita et al., 2012; Cheng et al., 2013; Nady et al., 2011).

These similarities imply that the binding of the TTD to its various interactors must be mutually exclusive—something we have verified for H3K9me3 (Figure 4)—raising the question of how LIG1 can outcompete the other binders. Indeed, $L2_{UHRF1}$ and $spacer_{UHRF1}$ form with the TTD intramolecular interactions, which should have a much higher probability of contact, especially at lower UHRF1 concentrations. As for H3K9me3 molecules, they form intermolecular interactions with the TTD, but they outnumber LIG1 by a factor of ~100 (Ferry et al., 2017). To be able to engage the TTD, it is expected that LIG1 should have an affinity significantly higher than the other binders, and this is in fact what we observe (Ferry et al., 2017). In the crystal structure, Arg122 and Arg125 of LIG1 formed interactions not seen for H3K9me3, $L2_{UHRF1}$, or $spacer_{UHRF1}$. Based on these observations, it seems likely that the high avidity of LIG1 for the TTD results from a combination of several hydrophilic and hydrophobic interactions that are not formed by the other binders.

Possible Modes of Regulation

The interaction between LIG1 and UHRF1 shows high affinity *in vitro*, and is easily detectable in cells. Nevertheless, it seems likely that the complex should undergo dissociation at some points in time and space, so that LIG1 can fulfill its catalytic activity—the ligation of Okazaki fragments—while UHRF1 remains on replicated DNA to ensure H3 ubiquitylation, DNMT1 recruitment, and allosteric DNMT1 activation (Bashtrykov et al., 2014; Berkyurek et al., 2014; Ishiyama et al., 2017; Nishiyama et al., 2013; Qin et al., 2015). How may the interaction between LIG1 and UHRF1 be dissociated?

A first and obvious way to dissociate the complex is to demethylate LIG1K126. Of note, ~80% of LIG1 molecules carry Lys126 methylation in cells (Ferry et al., 2017), suggesting that if Lys126 demethylation occurs it is a transient event. Future work may reveal if such an event occurs, and which enzyme is involved.

Our data reveal at least three additional possibilities to negatively regulate the UHRF1/LIG1 interaction. The first possibility is methylation of LIG1R121, which is predicted to disrupt the key electrostatic interactions with UHRF1D142. The second possibility is methylation of LIG1R125, which is predicted to prevent G9a from methylating LIG1K126 (Rathert et al., 2008), and should therefore phenocopy our LIG1R125A mutation. In this regard, FEN1, the flap endonuclease acting just before LIG1 during replication, is regulated by arginine methylation (Guo et al., 2010), and it could be of interest in the future to ask whether LIG1 is also targeted on Arg121 and Arg125 by arginine methyltransferases. Finally, a third event that may disrupt UHRF1/LIG1 complexes is phosphorylation of LIG1T123; we experimentally showed that it decreases affinity for the TTD ~10,000-fold. Interestingly, this mechanism could be conserved between interactions, as phosphorylation of the equivalent residues (Thr6 in H3, Ser298 in $L2_{UHRF1}$, and Ser651 in $spacer_{UHRF1}$) has a similar effect (Arita et al., 2012; Fang et al., 2016; Rothbart et al., 2012). We find that PKCβ, which is known to phosphorylate H3T6 (Metzger et al., 2010), efficiently phosphorylates LIG1T123, irrespective of the methylation status of LIG1K126, thus this kinase is a candidate that might regulate the dissociation of the UHRF1/LIG1 complex in cells. Interestingly, it has previously been observed that activation of PKC decreases DNA methylation (Lavoie et al., 2011).

LIG1 Modifies the Overall Structure of UHRF1: Functional Consequences

Several reports have unambiguously established that full-length UHRF1 undergoes intramolecular interactions, causing it to present a compact physical aspect, and leading to the inhibition of its molecular activities (Fang et al., 2016; Gelato et al., 2014; Harrison et al., 2016; Vaughan et al., 2018). Using SEC-SAXS and HS-AFM, we confirm that UHRF1 is compact, and further observe that its conformation becomes more extended and more dynamic once it interacts with LIG1. Therefore, LIG1 can be added to phosphatidylinositol 5-phosphate, hemimethylated DNA, and H3K9me3 (Fang et al., 2016; Gelato et al., 2014; Harrison et al., 2016) as a binder that affects the overall UHRF1 structure.

In spite of this similarity, LIG1 also presents a key difference with H3K9me3 with respect to its effect on the TTD and PHD domains. Indeed these two domains can form a functional module, in which the PHD is precisely positioned relative to the TTD by $L2_{UHRF1}$, which binds the TTD groove. The addition of H3K9me3 does not disrupt this architecture: instead H3K9me3 adopts a constrained conformation so that its N-terminus binds the PHD, and its C-terminus binds the TTD (Arita et al., 2012; Rothbart et al., 2013). In clear contrast, our SEC-SAXS experiments show that LIG1 does modify the TTD-PHD module, toward a more open conformation; presumably this happens by displacing $L2_{UHRF1}$ from the groove. Our ITC experiments also show that the PHD does not detectably bind the LIG1 peptide, and this is consistent with expectations as LIG1 does not have the free N-terminal ^{1}ARTK^{4} motif that is critical for interaction with the PHD (Arita et al., 2012; Hu et al., 2011; Lallous et al., 2011; Rajakumara et al., 2011). Our data show that, when UHRF1 is bound to LIG1, the PHD domain is free to bind H3K9me0 and H3K9me3, with similar affinities. Interestingly, we also find that, once the TTD-PHD is bound to H3K9me3, LIG1K126me3 can no longer bind. This mechanism could possibly ensure a unidirectional handing-over of UHRF1 from LIG1 to H3K9me3 behind the replication fork. These complex dynamics may be necessary to order, in space and time, the different functions that UHRF1 has to fulfill: recruitment to recently replicated DNA, methylation of histones, and activation of DNMT1.

Taken together, our results contribute to a better understanding of the critical epigenetic regulator UHRF1, and will guide future experiments to further study its functions. More generally, they provide an example of the flexibility deployed by structural domains in the recognition of methylated peptides, of the complex intermolecular and intramolecular events modulating protein structure, and of how these properties are used biologically.

STAR★METHODS

Detailed methods are provided in the online version of this paper and include the following:

- KEY RESOURCES TABLE
- CONTACT FOR REAGENT AND RESOURCE SHARING
- EXPERIMENTAL MODEL AND SUBJECT DETAILS
- METHOD DETAILS
  - Peptide Preparation
  - Crystallography of TTD and Its Complex with LIG1K126me3 Peptide
  - ITC Measurements
  - Fluorescent Three-Hybrid Assay (F3H)
  - *In Vitro* Methylation Assay
  - *In Vitro* Phosphorylation Assay
  - SEC-SAXS
  - HS-AFM Observations
  - Analysis of AFM Images
- QUANTIFICATION AND STATISTICAL ANALYSIS
- DATA AND SOFTWARE AVAILABILITY

SUPPLEMENTAL INFORMATION

Supplemental Information includes eight figures, one table, and three videos and can be found with this article online at https://doi.org/10.1016/j.str.2018.11.012.

ACKNOWLEDGMENTS

We would like to thank the beamline staff at the Photon Factory for X-ray data collection. We also thank Dr. T. Uchihashi for 2D-correlation coefficients analysis of HS-AFM. PAD thanks Allison Bardin for useful comments on the manuscript. We express our thanks to Dr. David Spector for sharing the BHK-LacOp cells. This study was supported by a PRESTO (14530337) from JST and MEXT, Grant-in-Aid for Scientific Research (B), 18H02392, (to K.A.). P.A.D. was supported by Association pour la Recherche contre le Cancer (ARC2014), by Agence Nationale de la Recherche (ANR-15-CE12-0012-01 and ANR-11-LABX-0071 under ANR-11-IDEX-0005-01), and by Institut National Du Cancer (INCa PLBio 2015-1-PLBio-01-DR A-1).

AUTHOR CONTRIBUTIONS

K.A. and P.-A.D. conceived the study and experimental design, analyzed experiments and co-wrote the manuscript. S.K., S.M., R.M., and K.A. analyzed the structural basis of the TTD:LIG1K126me3 complex. S.K., T.J., T.O., M.S., and K.A. performed SAXS measurements and analyzed the data. S.K., S.M., R.M., and K.A. analyzed interaction between TTD and LIG1 by ITC. L.F. and P.A.D. performed F3H assay. S.K., N.K., T.A., and K.A. performed HS-AFM experiments and analyzed the data. T.T., N.D., and Y.S. performed *in vitro* methylation assay.

DECLARATION OF INTERESTS

The authors declare no competing interests.

Received: September 13, 2018
Revised: October 19, 2018
Accepted: November 28, 2018
Published: January 10, 2019

REFERENCES

Afonine, P.V., Grosse-Kunstleve, R.W., Echols, N., Headd, J.J., Moriarty, N.W., Mustyakimov, M., Terwilliger, T.C., Urzhumtsev, A., Zwart, P.H., and Adams, P.D. (2012). Towards automated crystallographic structure refinement with phenix.refine. Acta Crystallogr. D Biol. Crystallogr. *68*, 352–367.

Allis, C.D., and Jenuwein, T. (2016). The molecular hallmarks of epigenetic control. Nat. Rev. Genet. *17*, 487–500.

Ando, T., Kodera, N., Takai, E., Maruyama, D., Saito, K., and Toda, A. (2001). A high-speed atomic force microscope for studying biological macromolecules. Proc. Natl. Acad. Sci. U S A *98*, 12468–12472.

Ando, T., Uchihashi, T., Kodera, N., Yamamoto, D., Miyagi, A., Taniguchi, M., and Yamashita, H. (2008). High-speed AFM and nano-visualization of biomolecular processes. Pflugers Archiv. *456*, 211–225.

Arita, K., Ariyoshi, M., Tochio, H., Nakamura, Y., and Shirakawa, M. (2008). Recognition of hemi-methylated DNA by the SRA protein UHRF1 by a base-flipping mechanism. Nature *455*, 818–821.

Arita, K., Isogai, S., Oda, T., Unoki, M., Sugita, K., Sekiyama, N., Kuwata, K., Hamamoto, R., Tochio, H., Sato, M., et al. (2012). Recognition of modification status on a histone H3 tail by linked histone reader modules of the epigenetic regulator UHRF1. Proc. Natl. Acad. Sci. U S A *109*, 12950–12955.

Avvakumov, G.V., Walker, J.R., Xue, S., Li, Y., Duan, S., Bronner, C., Arrowsmith, C.H., and Dhe-Paganon, S. (2008). Structural basis for recognition of hemi-methylated DNA by the SRA domain of human UHRF1. Nature *455*, 822–825.

Bashtrykov, P., Jankevicius, G., Jurkowska, R.Z., Ragozin, S., and Jeltsch, A. (2014). The UHRF1 protein stimulates the activity and specificity of the maintenance DNA methyltransferase DNMT1 by an allosteric mechanism. J. Biol. Chem. *289*, 4106–4115.

Berkyurek, A.C., Suetake, I., Arita, K., Takeshita, K., Nakagawa, A., Shirakawa, M., and Tajima, S. (2014). The DNA methyltransferase Dnmt1 directly interacts with the SET and RING finger-associated (SRA) domain of the multifunctional protein Uhrf1 to facilitate accession of the catalytic center to hemi-methylated DNA. J. Biol. Chem. *289*, 379–386.

Bostick, M., Kim, J.K., Esteve, P.-O., Clark, A., Pradhan, S., and Jacobsen, S.E. (2007). UHRF1 plays a role in maintaining DNA methylation in mammalian cells. Science *317*, 1760–1764.

Botuyan, M.V., Lee, J., Ward, I.M., Kim, J.-E., Thompson, J.R., Chen, J., and Mer, G. (2006). Structural basis for the methylation state-specific recognition of histone H4-K20 by 53BP1 and Crb2 in DNA repair. Cell *127*, 1361–1373.

Carr, S.M., Munro, S., Zalmas, L.-P., Fedorov, O., Johansson, C., Krojer, T., Sagum, C.A., Bedford, M.T., Oppermann, U., and La Thangue, N.B. (2014). Lysine methylation-dependent binding of 53BP1 to the pRb tumor suppressor. Proc. Natl. Acad. Sci. U S A *111*, 11341–11346.

Cheng, J., Yang, Y., Fang, J., Xiao, J., Zhu, T., Chen, F., Wang, P., Li, Z., Yang, H., and Xu, Y. (2013). Structural insight into coordinated recognition of trimethylated histone H3 lysine 9 (H3K9me3) by the plant homeodomain (PHD) and tandem tudor domain (TTD) of UHRF1 (ubiquitin-like, containing PHD and RING finger domains, 1) protein. J. Biol. Chem. *288*, 1329–1339.

Du, X., Li, Y., Xia, Y.-L., Ai, S.-M., Liang, J., Sang, P., Ji, X.-L., and Liu, S.-Q. (2016). Insights into protein-ligand interactions: mechanisms, models, and methods. Int. J. Mol. Sci. *17*, 144.

Emsley, P., Lohkamp, B., Scott, W.G., and Cowtan, K. (2010). Features and development of *Coot*. Acta Crystallogr. D Biol. Crystallogr. *66*, 486–501.

Evans, P.R., and Murshudov, G.N. (2013). How good are my data and what is the resolution? Acta Crystallogr. D Biol. Crystallogr. *69*, 1204–1214.

Fang, J., Cheng, J., Wang, J., Zhang, Q., Liu, M., Gong, R., Wang, P., Zhang, X., Feng, Y., Lan, W., et al. (2016). Hemi-methylated DNA opens a closed conformation of UHRF1 to facilitate its histone recognition. Nat. Commun. *7*, 11197.

Ferry, L., Fournier, A., Tsusaka, T., Adelmant, G., Shimazu, T., Matano, S., Kirsh, O., Amouroux, R., Dohmae, N., Suzuki, T., et al. (2017). Methylation of DNA ligase 1 by G9a/GLP recruits UHRF1 to replicating DNA and regulates DNA methylation. Mol. Cell *67*, 550–565.e5.

Franke, D., and Svergun, D.I. (2009). *DAMMIF*, a program for rapid *ab-initio* shape determination in small-angle scattering. J. Appl. Crystallogr. *42*, 342–346.

Gao, L., Tan, X.-F., Zhang, S., Wu, T., Zhang, Z.-M., Ai, H., and Song, J. (2018). An Intramolecular interaction of UHRF1 reveals dual control for its histone association. Structure *26*, 304–311.e3.

Gelato, K.A., Tauber, M., Ong, M.S., Winter, S., Hiragami-Hamada, K., Sindlinger, J., Lemak, A., Bultsma, Y., Houliston, S., Schwarzer, D., et al. (2014). Accessibility of different histone H3-binding domains of UHRF1 is allosterically regulated by phosphatidylinositol 5-phosphate. Mol. Cell *54*, 905–919.

Guo, Z., Zheng, L., Xu, H., Dai, H., Zhou, M., Pascua, M.R., Chen, Q.M., and Shen, B. (2010). Methylation of FEN1 suppresses nearby phosphorylation and facilitates PCNA binding. Nat. Chem. Biol. *6*, 766–773.

Harrison, J.S., Cornett, E.M., Goldfarb, D., DaRosa, P.A., Li, Z.M., Yan, F., Dickson, B.M., Guo, A.H., Cantu, D.V., Kaustov, L., et al. (2016). Hemi-methylated DNA regulates DNA methylation inheritance through allosteric activation of H3 ubiquitylation by UHRF1. Elife *5*, https://doi.org/10.7554/eLife.17101.

Hashimoto, H., Horton, J.R., Zhang, X., Bostick, M., Jacobsen, S.E., and Cheng, X. (2008). The SRA domain of UHRF1 flips 5-methylcytosine out of the DNA helix. Nature *455*, 826–829.

Herce, H.D., Deng, W., Helma, J., Leonhardt, H., and Cardoso, M.C. (2013). Visualization and targeted disruption of protein interactions in living cells. Nat. Commun. *4*, 2660.

Houliston, R.S., Lemak, A., Iqbal, A., Ivanochko, D., Duan, S., Kaustov, L., Ong, M.S., Fan, L., Senisterra, G., Brown, P.J., et al. (2017). Conformational dynamics of the TTD-PHD histone reader module of UHRF1 reveals multiple histone binding states, allosteric regulation and druggability. J. Biol. Chem. *292*, 20947–20959.

Hu, L., Li, Z., Wang, P., Lin, Y., and Xu, Y. (2011). Crystal structure of PHD domain of UHRF1 and insights into recognition of unmodified histone H3 arginine residue 2. Cell Res. *21*, 1374–1378.

Ishiyama, S., Nishiyama, A., Saeki, Y., Moritsugu, K., Morimoto, D., Yamaguchi, L., Arai, N., Matsumura, R., Kawakami, T., Mishima, Y., et al. (2017). Structure of the Dnmt1 reader module complexed with a unique two--mono-ubiquitin mark on histone H3 reveals the basis for DNA methylation maintenance. Mol. Cell *68*, 350–360.e7.

Kabsch, W. (2010). XDS. Acta Crystallogr. D Biol. Crystallogr. *66*, 125–132.

Konarev, P.V., Volkov, V.V., Sokolova, A.V., Koch, M.H.J., and Svergun, D.I. (2003). *PRIMUS*: a Windows PC-based system for small-angle scattering data analysis. J. Appl. Crystallogr *36*, 1277–1282.

Lallous, N., Legrand, P., McEwen, A.G., Ramón-Maiques, S., Samama, J.-P., and Birck, C. (2011). The PHD finger of human UHRF1 reveals a new subgroup of unmethylated histone H3 tail readers. PLoS One *6*, e27599.

Lavoie, G., Estève, P.-O., Laulan, N.B., Pradhan, S., and St-Pierre, Y. (2011). PKC isoforms interact with and phosphorylate DNMT1. BMC Biol. *9*, 31.

Liu, X., Gao, Q., Li, P., Zhao, Q., Zhang, J., Li, J., Koseki, H., and Wong, J. (2013). UHRF1 targets DNMT1 for DNA methylation through cooperative binding of hemi-methylated DNA and methylated H3K9. Nat. Commun. *4*, 1563.

McCoy, A.J., Grosse-Kunstleve, R.W., Adams, P.D., Winn, M.D., Storoni, L.C., and Read, R.J. (2007). Phaser crystallographic software. J. Appl. Crystallogr. *40*, 658–674.

Metzger, E., Imhof, A., Patel, D., Kahl, P., Hoffmeyer, K., Friedrichs, N., Müller, J.M., Greschik, H., Kirfel, J., Ji, S., et al. (2010). Phosphorylation of histone H3T6 by PKCbeta(I) controls demethylation at histone H3K4. Nature *464*, 792–796.

Nady, N., Lemak, A., Walker, J.R., Avvakumov, G.V., Kareta, M.S., Achour, M., Xue, S., Duan, S., Allali-Hassani, A., Zuo, X., et al. (2011). Recognition of multivalent histone states associated with heterochromatin by UHRF1 protein. J. Biol. Chem. *286*, 24300–24311.

Ngo, K.X., Kodera, N., Katayama, E., Ando, T., and Uyeda, T.Q. (2015). Cofilin-induced unidirectional cooperative conformational changes in actin filaments revealed by high-speed atomic force microscopy. Elife *4*, https://doi.org/10.7554/eLife.04806.

Nishiyama, A., Yamaguchi, L., Sharif, J., Johmura, Y., Kawamura, T., Nakanishi, K., Shimamura, S., Arita, K., Kodama, T., Ishikawa, F., et al. (2013). Uhrf1-dependent H3K23 ubiquitylation couples maintenance DNA methylation and replication. Nature *502*, 249–253.

Orthaber, D., Bergmann, A., and Glatter, O. (2000). SAXS experiments on absolute scale with Kratky systems using water as a secondary standard. J. Appl. Cryst. *33*, 218–225.

Qin, W., Wolf, P., Liu, N., Link, S., Smets, M., La Mastra, F., Forné, I., Pichler, G., Hörl, D., Fellinger, K., et al. (2015). DNA methylation requires a DNMT1 ubiquitin interacting motif (UIM) and histone ubiquitination. Cell Res. *25*, 911–929.

Rajakumara, E., Wang, Z., Ma, H., Hu, L., Chen, H., Lin, Y., Guo, R., Wu, F., Li, H., Lan, F., et al. (2011). PHD finger recognition of unmodified histone H3R2 links UHRF1 to regulation of euchromatic gene expression. Mol. Cell *43*, 275–284.

Rathert, P., Dhayalan, A., Murakami, M., Zhang, X., Tamas, R., Jurkowska, R., Komatsu, Y., Shinkai, Y., Cheng, X., and Jeltsch, A. (2008). Protein lysine methyltransferase G9a acts on non-histone targets. Nat. Chem. Biol. *4*, 344–346.

Rothbart, S.B., Krajewski, K., Nady, N., Tempel, W., Xue, S., Badeaux, A.I., Barsyte-Lovejoy, D., Martinez, J.Y., Bedford, M.T., Fuchs, S.M., et al. (2012). Association of UHRF1 with methylated H3K9 directs the maintenance of DNA methylation. Nat. Struct. Mol. Biol. *19*, 1155–1160.

Rothbart, S.B., Dickson, B.M., Ong, M.S., Krajewski, K., Houliston, S., Kireev, D.B., Arrowsmith, C.H., and Strahl, B.D. (2013). Multivalent histone engagement by the linked tandem Tudor and PHD domains of UHRF1 is required for the epigenetic inheritance of DNA methylation. Genes Dev. *27*, 1288–1298.

Schübeler, D. (2015). Function and information content of DNA methylation. Nature *517*, 321–326.

Sharif, J., Muto, M., Takebayashi, S., Suetake, I., Iwamatsu, A., Endo, T.A., Shinga, J., Mizutani-Koseki, Y., Toyoda, T., Okamura, K., et al. (2007). The SRA protein Np95 mediates epigenetic inheritance by recruiting Dnmt1 to methylated DNA. Nature *450*, 908–912.

Shimizu, N., Yatabe, K., Nagatani, Y., Saijyo, S., Kosuge, T., and Igarashi, N. (2016). Software development for analysis of small-angle X-ray scattering data. In AIP Conference Proceedings, (AIP Publishing LLC), p. 050017.

Smets, M., Link, S., Wolf, P., Schneider, K., Solis, V., Ryan, J., Meilinger, D., Qin, W., and Leonhardt, H. (2017). DNMT1 mutations found in HSANIE patients affect interaction with UHRF1 and neuronal differentiation. Hum. Mol. Genet. *26*, 1522–1534.

Tachibana, M., Sugimoto, K., Fukushima, T., and Shinkai, Y. (2001). Set domain-containing protein, G9a, is a novel lysine-preferring mammalian histone methyltransferase with hyperactivity and specific selectivity to lysines 9 and 27 of histone H3. J. Biol. Chem. *276*, 25309–25317.

Tong, Q., Cui, G., Botuyan, M.V., Rothbart, S.B., Hayashi, R., Musselman, C.A., Singh, N., Appella, E., Strahl, B.D., Mer, G., et al. (2015). Structural plasticity of methyllysine recognition by the tandem Tudor domain of 53BP1. Structure *23*, 312–321.

Uchihashi, T., Iino, R., Ando, T., and Noji, H. (2011). High-speed atomic force microscopy reveals rotary catalysis of rotorless F1-ATPase. Science *333*, 755–758.

Uchihashi, T., Kodera, N., and Ando, T. (2012). Guide to video recording of structure dynamics and dynamic processes of proteins by high-speed atomic force microscopy. Nat. Protoc. *7*, 1193–1206.

Vaughan, R.M., Dickson, B.M., Cornett, E.M., Harrison, J.S., Kuhlman, B., and Rothbart, S.B. (2018). Comparative biochemical analysis of UHRF proteins reveals molecular mechanisms that uncouple UHRF2 from DNA methylation maintenance. Nucleic Acids Res. *46*, 4405–4416.

Volkov, V.V., and Svergun, D.I. (2003). Uniqueness of *ab initio* shape determination in small-angle scattering. J. Appl. Cryst. *36*, 860–864.

von Meyenn, F., Iurlaro, M., Habibi, E., Liu, N.Q., Salehzadeh-Yazdi, A., Santos, F., Petrini, E., Milagre, I., Yu, M., Xie, Z., et al. (2016). Impairment of DNA methylation maintenance is the main cause of global demethylation in naive embryonic stem cells. Mol. Cell *62*, 848–861.

Zhao, Q., Zhang, J., Chen, R., Wang, L., Li, B., Cheng, H., Duan, X., Zhu, H., Wei, W., Li, J., et al. (2016). Dissecting the precise role of H3K9 methylation in crosstalk with DNA maintenance methylation in mammals. Nat. Commun. *7*, 12464.

STAR★METHODS

KEY RESOURCES TABLE

REAGENT or RESOURCE	SOURCE	IDENTIFIER
Bacterial and Virus Strains		
E.Coli Rosetta™ 2 (DE3)	Novagen	Cat#71400-3CN
Chemicals, Peptides, and Recombinant Proteins		
Recombinant UHRF1 TTD (residues 123-285)	Arita et al. (2012)	N/A
Recombinant UHRF1 vTTD (residues 123-285 Δ167-175)	This study	N/A
Recombinant UHRF1 TTD D142A (residues 123-285)	Ferry et al. (2017)	N/A
Recombinant UHRF1 TTD Y188A/Y191A (residues 123-285)	Ferry et al. (2017)	N/A
Recombinant UHRF1 TTD E193A (residues 123-285)	This study	N/A
Recombinant UHRF1 TTD E276A (residues 123-285)	This study	N/A
Recombinant UHRF1 TTD W238A (residues 123-285)	This study	N/A
Recombinant UHRF1 PHD (residues 299-366)	Arita et al. (2012)	N/A
Recombinant UHRF1 TTD-PHD (residues 123-366)	Arita et al. (2012)	N/A
Recombinant UHRF1 TTD-PHD D142A (residues 123-366)	This study	N/A
Recombinant UHRF1 TTD-PHD Y188A/Y191A (residues 123-366)	This study	N/A
Recombinant UHRF1 TTD-PHD D334A/D337A (residues 123-366)	This study	N/A
Recombinant full length His-tagged UHRF1	Nishiyama et al. (2013)	N/A
Recombinant full length His-tagged UHRF1 D142A	This study	N/A
Chemical synthesized LIG1K126me3 (residues 118-130)	Ferry et al. (2017)	N/A
Chemical synthesized LIG1K126me0 (residues 118-130)	Ferry et al. (2017)	N/A
Chemical synthesized LIG1R121A (residues 118-130)	This study	N/A
Chemical synthesized LIG1T123ph (residues 118-130)	This study	N/A
Chemical synthesized LIG1R125A (residues 118-130)	This study	N/A
Chemical synthesized LIG1R121A/K126me3 (residues 118-130)	This study	N/A
Chemical synthesized LIG1T123ph/K126me3 (residues 118-130)	This study	N/A
Chemical synthesized LIG1R125A/K126me3 (residues 118-130)	This study	N/A
Chemical synthesized H3K9me3 (residues 1-12)	Arita et al. (2012)	N/A
Chemical synthesized H3K4R/K9me3 (residues 1-12)	This study	N/A
Chemical synthesized H3Q5R/K9me3 (residues 1-12)	This study	N/A
Chemical synthesized H3K4R/Q5R/K9me3 (residues 1-12)	This study	N/A
Recombinant GST-SENP protease	Arita et al. (2008)	N/A
PreScission protease	GE Healthcare	Cat#27084301
Recombinant G9a	Tachibana et al. (2001)	N/A
Recombinant GLP	Tachibana et al. (2001)	N/A
Recombinant human PKCβ2 protein	abcam	Cat#ab60841
Critical Commercial Assays		
KOD-Plus Mutagenesis kit	Toyobo	Cat#SMK-101
Gibson Assembly Cloning kit	NEB	Cat#E5510

(*Continued on next page*)

Continued

REAGENT or RESOURCE	SOURCE	IDENTIFIER
Deposited Data		
Crystal structure of apo-TTD	This study	PDB: 5YYA
Crystal structure of TTD in complex with LIG1K126me3	This study	PDB: 5YY9
NMR structure of TTD in complex with H3K9me3	Nady et al. (2011)	PDB: 2L3R
Crystal structure of TTD in complex with H3K9me3	Nady et al. (2011)	PDB: 3DB3
Crystal structure of TTD-PHD in complex with H3K9me3	Arita et al. (2012)	PDB: 3ASK
Experimental Models: Cell Lines		
BHK-LacOp cells (Baby Hamster Kidney, female)	Herce et al. (2013)	N/A
Oligonucleotides		
Primer: UHRF1 Δ167-175 Forward: 5'-GCCCCCTCCCGGCCG GCGCTGGAGGAGGACGTCATT	Hokkaido System Science Co.,Ltd.	N/A
Primer: UHRF1 Δ167-175 Reverse:5'-CTCCAGCGCCGGCCG GGAGGGGGCCTTCCGCGTCAC	Hokkaido System Science Co.,Ltd.	N/A
Primer: UHRF1 E193A Forward: 5'-CTACCCGGCAAACGGCGT GGTCCAGATGAA	Hokkaido System Science Co.,Ltd.	N/A
Primer: UHRF1 E193A Reverse: 5'-CGCCGTTTGCCGGGTAGT CGTCGTATTTCA	Hokkaido System Science Co.,Ltd.	N/A
Primer: UHRF1 E276A Forward: 5'-CGTGGACGCAGTCTTCAA GATTGAGCGGCC	Hokkaido System Science Co.,Ltd.	N/A
Primer: UHRF1 E276A Reverse: 5'-TGAAGACTGCGTCCACGA AGATGATCCGAC	Hokkaido System Science Co.,Ltd.	N/A
Primer: UHRF1 W238A Forward: 5'-GGGCTTCGCGTACGACG CGGAGATCTCCAG	Hokkaido System Science Co.,Ltd.	N/A
Primer: UHRF1 W238A Reverse: 5'-CGTCGTACGCGAAGCCC CGCTCCTTGGGGT	Hokkaido System Science Co.,Ltd.	N/A
Primer: UHRF1 D334A/D337A Forward: 5'-TGTGCGCTGAGTG CGCCATGGCCTTCCACA	Hokkaido System Science Co.,Ltd.	N/A
Primer: UHRF1 D334A/D337A Reverse: 5'-CCATGGCGCACTC AGCGCACATGAGCTGCT	Hokkaido System Science Co.,Ltd.	N/A
Recombinant DNA		
pGEX-ST1-UHRF1 TTD WT (residues 123-285)	Arita et al., 2012	N/A
pGEX-ST1-UHRF1 vTTD (residues 123-285 Δ167-175)	This study	N/A
pGEX-ST1-UHRF1 TTD D142A (residues 123-285)	Ferry et al., 2017	N/A
pGEX-ST1-UHRF1 TTD Y188A/Y191A (residues 123-285)	Ferry et al., 2017	N/A
pGEX-ST1-UHRF1 TTD E193A (residues 123-285)	This study	N/A
pGEX-ST1-UHRF1 TTD E276A (residues 123-285)	This study	N/A
pGEX-ST1-UHRF1 TTD W238A (residues 123-285)	This study	N/A
pGEX-ST1-UHRF1 PHD WT (residues 299-366)	Arita et al., 2012	N/A
pGEX-ST1-UHRF1 TTD-PHD WT (residues 123-366)	Arita et al., 2012	N/A
pGEX-ST1-UHRF1 TTD-PHD D142A (residues 123-366)	This study	N/A
pGEX-ST1-UHRF1 TTD-PHD Y188A/Y191A (residues 123-366)	This study	N/A
pGEX-ST1-UHRF1 TTD-PHD D334A/D337A (residues 123-366)	This study	N/A
pGEX-6P-1-full length His-tagged UHRF1 WT	Nishiyama et al. (2013)	N/A
pGEX-6P-1-full length His-tagged UHRF1 D142A	This study	N/A
pEGFP-C2- full-length UHRF1 WT	Ferry et al. (2017)	PAD1543
pEGFP-C2- full-length UHRF1 D142A	This study	N/A
pEGFP-C2- full-length UHRF1 E193A	This study	N/A
pEGFP-C2- full-length UHRF1 E276A	This study	N/A
pEGFP-C2- full-length UHRF1 W238A	This study	N/A

(*Continued on next page*)

Continued

REAGENT or RESOURCE	SOURCE	IDENTIFIER
pmRFP-C2 Full-length human LIG1 WT	Ferry et al. (2017)	PAD1766
pmRFP-C2 Full-length human LIG1 R121A	This study	N/A
pmRFP-C2 Full-length human LIG1 T123D	This study	N/A
pmRFP-C2 Full-length human LIG1 R125A	This study	N/A
Software and Algorithms		
Coot	Emsley et al. (2010)	http://www2.mrc-lmb.cam.ac.uk/personal/pemsley/coot
PHENIX	Afonine et al. (2012)	https://www.phenix-online.org/documentation/index.html
PHASER	McCoy et al. (2007)	http://www-structmed.cimr.cam.ac.uk/phaser/
XDS	Kabsch (2010)	http://xds.mpimf-heidelberg.mpg.de/
AIMLESS	Evans and Murshudov (2013)	http://www.ccp4.ac.uk/html/aimless.html
Pymol	http://www.pymol.org	http://www.pymol.org
SAngler	Shimizu et al. (2016)	http://pfwww.kek.jp/saxs/SAngler.html
PRIMUS	Konarev et al., 2003	https://www.embl-hamburg.de/biosaxs/primus.html
DAMMIF	Franke and Svergun (2009)	https://www.embl-hamburg.de/biosaxs/dammif.html
DAMAVER & DAMMIN	Volkov and Svergun, 2003	https://www.embl-hamburg.de/biosaxs/damaver.html
Origin 5.0, 7.0 and Origin Pro 9.1		https://www.originlab.com/
Other		
Glutathione Sepharose 4B	GE Healthcare	Cat#17075605
HiTrap Heparin HP column	GE Healthcare	Cat#17040701
HiTrap Q HP column	GE Healthcare	Cat#17115401
HiLoad 26/600 Superdex 75 column	GE Healthcare	Cat#28989334
HiLoad 26/600 Superdex 200 column	GE Healthcare	Cat#28989336
Superdex 200 Increase 10/300 GL	GE Healthcare	Cat#28990944
Superdex 200 Increase 5/150 GL	GE Healthcare	Cat#28990945
RIGAKU R-AXIS IV++ with MicroMax 007	RIGAKU	
MicroCal VP-ITC Isothermal Titration Calorimeter	Malvern	Cat#MicroCal VP-ITC
Q Exactive mass spectrometer	Thermo Fisher Scientific	
MALDI-TOF/MS	Brucker: autoflex-YS	
Atomic force microscope	Ando et al., 2001, 2008	N/A
Cantilevers for AFM	Olympus	BL-AC10DS-A2

CONTACT FOR REAGENT AND RESOURCE SHARING

Further information and requests for resources and reagents should be directed to and will be fulfilled by the Lead Contact, Kyohei Arita (aritak@yokohama-cu.ac.jp)

EXPERIMENTAL MODEL AND SUBJECT DETAILS

All recombinant proteins (UHRF1 full-length, TTD, PHD and TTD-PHD) were expressed in *E. coli* Rosetta™ 2 (DE3) (Novagen). Cells were grown in Luria-Bertani (LB) medium at 37°C shaking at 150 rpm in an INNOVA® 42 shaker (New Brunswick Science) and induced with 0.2 mM isopropyl-β-D-thiogalactopyranoside (IPTG) when they reached an optical density of 0.6∼0.7 at 660 nm. The cells were incubated at 15°C overnight or 30°C for 6 hours.

For fluorescent-3-hybrid experiments, we used BHK cells (Baby Hamster Kidney cells, female, ATCC CCL-10), modified to contain multiple copies of the Lac Operator (Herce et al., 2013). The cells were grown in DMEM/10% Fetal Calf Serum and reverse-transfected in 24-well plates using Lipofectamine 2000 (ThermoFisher, Cat# 11668027).

METHOD DETAILS

Peptide Preparation

The human LIG1 (UniProt ID: P18858) peptides, residues 118-130 (NH^2-^{118}IPKRRTARKQLPK^{130}-COOH) harboring K126me3, R121A-K126me3, R125A-K126me3 or T123ph-K126me3, and histone H3K9me3 (NH^2-^{1}ARTKQTAR-K(me3)-STG^{12}-COOH), K4R-K9me3, Q5R-K9me3 and K4R-Q5R-K9me3 were purchased from Toray Research Center (Tokyo, Japan).

Crystallography of TTD and Its Complex with LIG1K126me3 Peptide

The TTD (residues 123-285) of human UHRF1 (UniProt ID: Q96T88) was expressed as a fusion protein with glutathione S-transferase (GST) and small ubiquitin like modifier-1 (SUMO) at its N-terminus (Arita et al., 2012). The protein was expressed in *E. coli* strain Rosetta^{TM} 2 (DE3) (Novagen). Cells were grown at 37°C in Luria-Bertani (LB) medium and induced with 0.2 mM isopropyl-β-D-thiogalactopyranoside (IPTG) when they reached an optical density (O.D.) of 0.6 at 660 nm, and incubated at 15°C for 15 hours. The cells were re-suspended with a lysis buffer (40 mM Tris-HCl (pH8.0), 300 mM NaCl, 0.5 mM tris(2-carboxyethyl)phosphine Hydrochloride (TCEP), 1 mM EDTA, 10% glycerol and protease inhibitor cocktail (Nacalai tesque, Cat# 03969-21)) and sonicated with the cycle of pulse on for 5 seconds and pulse off for 1 minute (total pulse on time; 5 minutes). Insoluble debris was removed by centrifugation at 19,000 rpm for 40 minutes at 4°C using Avanti J-E with a rotor JA-20 (BECKMAN COULTER). The GST-SUMO-tagged TTD was loaded to Glutathione Sepharose 4B (GS4B; GE Healthcare, Cat# 17075605), and the unbound proteins were washed by the lysis buffer. The GST-SUMO-tagged TTD was eluted by an elution buffer; 20 mM Tris-HCl (pH 8.0), 300 mM NaCl, 1 mM dithiothreitol (DTT), 10 % glycerol, 20 mM reduced glutathione (GSH). The GST-SUMO tag was cleaved by the SUMO specific protease, SENP (purified in house), at room temperature for 5∼6 hours. The TTD was further purified by anion-exchange chromatography, HiTrap Q (GE Healthcare, Cat# 17115401) using gradient elution from 100 – 500 mM NaCl in 20 mM Tris-HCl (pH 8.0) buffer containing 0.5 mM DTT and 10% glycerol. Finally, the protein was purified with Hiload 26/600 Superdex 75 size exclusion chromatography (GE Healthcare, Cat# 28989334) equilibrated with 20 mM Tris-HCl (pH 8.0), 150 mM NaCl and 0.2 mM DTT. Cocrystallization of this wild-type TTD with the LIG1K126me3 peptide was unsuccessful, so we used instead a modified version of the TTD, designated vTTD, deleting residues 167-175. The protocols of cell culture and purification of vTTD are the same as for wild-type TTD.

Crystal of apo-TTD were obtained by using a reservoir solution containing 0.1 M Bis-Tris (pH 6.5), 200 mM ammonium acetate and 25% (w/v) polyethylene glycol (PEG) 3,350 at 4°C. The crystals were cryoprotected by 20% (v/v) ethylene glycol. Diffraction data were collected at a wavelength of 1.5418 Å on a RIGAKU R-AXIS IV^{++} equipped with MicroMax 007 (RIGAKU). Data were processed with program XDS package (Kabsch, 2010) and AIMLESS (Evans and Murshudov, 2013) at 1.7 Å resolution. Data were processed in space group $P2_12_12_1$ and Matthews coefficient suggested one molecule of apo-TTD in the asymmetric unit. The structure of apo-TTD was solved by molecular replacement method using the coordinates of the human UHRF1 TTD (PDB; 3DB3 (Nady et al., 2011)) as a search model. Molecular replacement and model refinement were performed using PHASER (McCoy et al., 2007) and PHENIX (Afonine et al., 2012), respectively. After rigid body refinement and simulated annealing by PHENIX, $2|F_o| - |F_c|$ difference Fourier map corresponding to the flexible loop, residues 160-179, was unambiguously observed, which has not seen in search model. Manual model building was performed with Coot (Emsley et al., 2010). After several cycles of refinement with PHENIX, the model converged well at 1.7 Å resolution with a crystallographic *R*-factor of 17.2 % and free *R*-factor of 20.6%.

The vTTD:LIG1K126me3 complex was prepared by adding a 1.5-molar excess of the LIG1K126me3 peptide to the protein before concentration using an Amicon concentrator with a 10,000 Da cutoff (Millipore). The crystal was obtained using a 30 mg/ml concentration of the complex at 20°C and the hanging drop vapor diffusion method with a reservoir solution containing 100 mM Tris-HCl (pH 7.0), 200 mM tri-potassium phosphate and 20% (w/v) PEG3,350. The crystal was directly frozen in liquid nitrogen using a cryoprotectant containing 20% (v/v) ethylene glycol. The X-ray diffraction data were collected at a wavelength of 0.98000 Å on a Pilatus3 6M detector in beam line BL-17A at Photon Factory (Tsukuba, Japan) and scaled at 2.65 Å resolution with the program XDS package and Aimless. Data were processed in space group $P2_12_12_1$ and Matthews coefficient suggested two molecules of vTTD:LIG1K126me3 complex in the asymmetric unit. Molecular replacement was performed by PHASER using apo-TTD structure determined in this study as a search model. Manual model building was performed with Coot. After rigid body refinement and simulated annealing by PHENIX, $2|F_o| - |F_c|$ difference Fourier map corresponding to LIG1K126me3 were unambiguously observed. After several cycle of model refinement by PHENIX, the final model converged at 2.65 Å resolution with a crystallographic *R*-factor of 23.1% and a free *R*-factor of 28.8%. The crystallographic data and refinement statistics are given in Table 1. The figures were generated using Pymol (http://www.pymol.org).

ITC Measurements

Human UHRF1 PHD (residues 299-366) and TTD-PHD (residues 123-366) were expressed as GST-SUMO fusion protein and purified in the same experimental conditions. The proteins were expressed in *E. coli* strain Rosetta^{TM} 2 (DE3). The protein expression was induced with 0.2 mM IPTG at $O.D_{660}$ = 0.6∼0.7. In the case of the PHD, the cells were incubated at 30°C for 6 hours; for the TTD-PHD, the cells were incubated at 15°C for 15 hours. The cells were re-suspended with a lysis buffer (40 mM Tris-HCl (pH8.0), 300 mM NaCl, 0.5 mM TCEP, 30 μM zinc acetate, 10% glycerol and protease inhibitor cocktail) and sonicated with the same cycle

as TTD. Insoluble debris was removed by centrifugation at 19,000 rpm for 40 minutes at 4°C. The GST-SUMO-tagged protein was loaded to GS4B and eluted by the elution buffer: 20 mM Tris-HCl (pH 8.0), 300 mM NaCl, 1 mM DTT, 10 % glycerol, 20 mM GSH. The GST-SUMO tag was cleaved by the SENP at room temperature for 5∼6 hours. The TTD-PHD or PHD was further purified by anion-exchange chromatography, HiTrap Q using gradient elution from 100 -500 mM NaCl in 20 mM Tris-HCl (pH 8.0) buffer containing 0.5 mM DTT and 10% glycerol. Finally, the protein was purified with Hiload 26/600 Superdex 75 size exclusion chromatography equilibrated with 10 mM Tris-HCl (pH 8.0), 150 mM NaCl and 0.2 mM TCEP. For binding experiments, we introduced the following mutations in the context of WT TTD (residues 123-285): D142A, Y188A/Y191A, E193A, E276A, W238A. We also introduced the following mutations within the TTD-PHD: D142A, Y188A/Y191A, D334A/D337A. All the constructs were obtained by the Quickchange mutagenesis method (Agilent Technologies).

Purified UHRF1 WT TTD, mutants of the TTD (D142A, Y188A/Y191A, E193A, E276A, W238A), vTTD, PHD, TTD-PHD, and mutants of the TTD-PHD (D142A, Y188A/Y191A, D334A/D337A) were buffer-exchanged using Superdex 200 Increase 10/300 GL (GE Healthcare, Cat# 28990944) equilibrated with the ITC buffer (10 mM HEPES-NaOH (pH 7.5), 150 mM NaCl, 0.25 mM TCEP). Lyophilized LIG1 peptides (residues 118-130) and H3K9me3 peptide (residues 1-12) were dissolved in the ITC buffer. A MicroCal LLC calorimeter, VP-ITC (MicroCal), was used for the ITC measurements. The 10∼20 μM of protein solution in the calorimetric cell was titrated with the 125∼250 μM of peptide solution at 293 K. The data were analyzed with the software ORIGIN (MicroCal) using a one-site model. The first data point was excluded from the analysis. For each interaction, we performed at least three independent experiments.

Fluorescent Three-Hybrid Assay (F3H)

The starting plasmids for F3H were: full-length human UHRF1 cloned in pEGFP-C2 (plasmid PAD1543) (Ferry et al., 2017) and full-length human LIG1, cloned in pmRFP-C2 (plasmid PAD1766) (Ferry et al., 2017). The various mutations (UHRF1 D142A, E193A, E276A, W238A; LIG1 R121A, T123D, R125A) were introduced by Gibson Assembly Cloning. The F3H assay were performed as previously described (Herce et al., 2013): we used BHK cells containing multiple copies of the Lac Operator (a kind gift of David Spector and Heinrich Leonhardt). The cells were grown in DMEM/10% Fetal Calf Serum and reverse-transfected in 24-well plates using Lipofectamine 2000. Each well received equal amounts of three plasmids encoding: the LacR-GFP binder fusion protein (plasmid kindly given by Heinrich Leonhardt), the GFP-UHRF1 fusion (or its mutant derivatives), and the LIG1-mRFPC2 fusion (or its mutant derivatives). Eighteen hours after transfection, the coverslips were washed with PBS, fixed with 4% paraformaldehyde (10 minutes, room temperature), permeabilized with 0.5% Triton X-100 in PBS (4 minutes at 4°C), and stained with DAPI. They were mounted and observed at 40X magnification on a fluorescence microscope. Cells expressing both GFP and RFP were scored for colocalization. Each experiment was carried out at least twice independently, with 100 cells scored in blind in each repetition.

In Vitro Methylation Assay

Methylation assays were performed in 50 mM Tris-HCl (pH 8.0), 10 μM LIG1 peptide (residues 118-130; WT, R121A, T123ph, R125A), 0.1 μg/ μL enzyme, 200 μM S-adenosyl-L-methionine at 30°C. The reactions were stopped by the addition of trifluoroacetic acid to 0.5%. Samples were then analyzed by mass spectrometry. Recombinant G9a and GLP were prepared as described previously (Tachibana et al., 2001). The following peptides were used: hLIG1(118-130) WT, IPKRRTARKQLPK; hLIG1(118-130) T123ph, IPKRRT(ph)ARKQLPK; hLIG1(118-130) R125A, IPKRRTAAKQLPK; hLIG1(118-130) R121A, IPKARTARKQLPK.

The samples of methylation assays were diluted to 1/100 with 0.1% formic acid and applied to nano-liquid chromatography-tandem mass spectrometry using a Q Exactive mass spectrometer (Thermo Fisher Scientific). The peptide mixtures (2 μL) were separated by nano ESI spray column (75 μm [ID] × 100 mm [L], NTCC analytical column C18, 3 μm, Nikkyo Technos) with a linear gradient of 0 - 35% buffer B (acetonitrile with 0.1% (v/v) formic acid) in buffer A (MilliQ water with 0.1% (v/v) formic acid) at a flow rate of 300 nL/min over 10 minutes (EAST-nLC 1000; Thermo Fisher Scientific). The mass spectrometer was operated in the positive-ion mode for MS and MS/MS, and the MS/MS spectra were acquired using an inclusion list containing methylation specific peptide ions (WT: triply charged none-, mono-, di- and tri-methyl IPKRRTARKQLPK ion m/z= 531.346, 536.018, 540.690 and 545.362, respectively. T123ph: triply charged none, mono-, di- and tri-methyl IPKRRT(ph)ARKQLPK ion m/z= 558.001, 562.673, 567.345 and 572.017, respectively. R125A and R121A: triply charged none-, mono-, di- and tri-methyl IPKRRTAAKQLPK and IPKARTARKQLPK ion m/z= 502.991, 507.663, 512.335 and 517.007, respectively.) The MS chromatograms of these peptide ions were drawn using Qual Browser, Thermo Xcalibur 3.1.66.10 and each peptide amount was estimated by the peak area.

In Vitro Phosphorylation Assay

Phosphorylation assays were performed in 20 mM HEPES-NaOH (pH 7.5), 1 mM DTT, 1 mM β-Glycerophosphate, 0.05 mM Na_3VO_4, 1 mM ATP, 10 mM $MgCl_2$, 10 μM LIG1 peptide (residues 118-130; WT and K126me3), 0.02 μg/ μL human PKCβ (Abcam, Cat# ab60841) at 30°C for 15 hours. Samples were then analyzed by MALDI-TOF/MS (Brucker: autoflex-YS).

SEC-SAXS

Protein preparation of the WT and D142A mutant of TTD-PHD, residues 123-366, were described as before. SAXS data were collected on Photon Factory BL10C (Tsukuba, Japan) using UPLC® ACQUITY (Waters) integrated SAXS set-up. 50 μl of 6 mg/ml sample was loaded onto a 15/150GL INCREASE Superdex 200 (GE Healthcare, Cat# 28990944, column volume; 3 ml) pre-equilibrated by 20 mM Tris-HCl (pH 7.5), 150 mM NaCl, 2 mM DTT, 10 μM zinc acetate and 5% glycerol at a flow rate of 0.25 ml/min

at 4°C. The flow rate was reduced at 0.025 ml/min at elution volume of 1.85-2.30 ml. X-ray scattering was collected every 20 seconds on a PILATUS3 2M detector over an angular range q_{min} = 0.00690 Å^{-1} to q_{max} = 0.27815 Å^{-1}. UV spectra at a range 200 nm to 450 nm was recoded every 10 seconds. Circular averaging and subtraction including radius of gyration R_g and $I(0)$ calculations were carried out using program SAnglar (Shimizu et al., 2016) to obtain one-dimensional scattering data $I(q)$ as a function of q ($q = 4\pi\sin\theta/\lambda$, where 2θ is the scattering angle and λ is the X-ray wavelength 1.5 Å). To obtain scattering intensity on an absolute scale, measured scattering intensities were calibrated based on a scattering intensity of water (Orthaber et al., 2000). Estimation of the molecular weight of samples was calculated from $I(q)$ data of bovine carbonic anhydrolase (Sigma) at the most highest value of $I(0)$. The radius of gyration R_g and forward scattering intensity $I(0)$ were estimated from the Guinier plot of $I(q)$ in the smaller angle region of $qR_g < 1.3$. The distance distribution function $P(r)$ of the sample at the highest peak of A_{280} and $I(0)$ was calculated in the program GNOM, where the experimental $I(q)$ data were used in a q-range from 0.00885 to 0.17670 Å^{-1}. The maximum particle dimension D_{max} was estimated from the $P(r)$ function as the distance r for which $P(r) = 0$. *ab initio* three-dimensional shape reconstruction was performed using the DAMMIF (Franke and Svergun, 2009). In total, 10 models were averaged and the resulting structures were compared with the crystal structure of TTD-PHD in complex with H3K9me3 (PDB: 3ASK) in PyMOL. The SAXS data statistics are given in Table S1.

HS-AFM Observations

N-terminal 6×histidine (His6) tag full-length human UHRF1 was sub-cloned into pGEX6P-1 (GE Healthcare, Cat# 28954648). The UHRF1 wild type and D142A mutant were expressed in *E. coli* Rosettta2 (DE3) and induced with 0.2 mM IPTG at $O.D_{660}$ = 0.7. The cells were further incubated at 15°C for 15 hours. The cells were re-suspended with a lysis buffer (40 mM Tris-HCl (pH8.0), 300 mM NaCl, 0.5 mM TCEP, 30 μM zinc acetate, 10% glycerol and protease inhibitor cocktail) and sonicated with the same cycle as TTD. Insoluble debris was removed by centrifugation at 19,000 rpm for 40 minutes at 4°C. The soluble proteins were loaded to GS4B and eluted by the elution buffer: 20 mM Tris-HCl (pH 8.0), 300 mM NaCl, 1 mM DTT, 10 % glycerol, 20 mM GSH. The GST tag was cleaved by the PreScission protease (GE Healthcare, Cat# 27084301) at 4°C for overnight. The UHRF1 was further purified by HiTrap Heparin (GE Healthcare, Cat# 17040701) using gradient elution from 150 - 800 mM NaCl in 20 mM Tris-HCl (pH 8.0) buffer containing 0.5 mM DTT and 10% glycerol. Finally, the protein was purified with Hiload 26/600 Superdex 200 size exclusion chromatography equilibrated with 10 mM Tris-HCl (pH 8.0), 500 mM NaCl, 10% glycerol 0.2 mM TCEP and 10 μM zinc acetate.

HS-AFM imaging was performed in solution at room temperature using a laboratory-built HS-AFM setup (Ando et al., 2001, 2008) as described previously (Uchihashi et al., 2012). In brief, a glass sample stage (diameter, 2 mm; height, 2 mm) with a thin mica disc (1 mm in diameter and ~0.05 mm thick) glued to the top by epoxy was attached onto the top of a Z-scanner by a drop of nail polish. A freshly cleaved mica surface was prepared by removing the top layers of mica using Scotch tape and coated by 2 μl of 5 mM $NiCl_2$. Then, a drop (2 μl) of diluted protein sample (ca. 3 nM) in dilution buffer (20 mM Tris-HCl (pH 7.5), 500 mM NaCl and 10% glycerol) was placed on the mica surface. After incubation for 3 minutes at room temperature, the mica surface was rinsed with 20 μl of the observation buffer (20 mM Tris-HCl (pH 7.5), 150 mM NaCl) to remove floating samples. The sample stage was then immersed in a liquid cell containing ~60 μl of the observation buffer with and without 150 nM LIG1K126me3 peptide. AFM Imaging was carried out in the tapping mode, using small cantilevers (Olympus, Cat# BL-AC10DS-A2); resonant frequency, ~0.5 MHz in water; quality factor, ~2 in water; spring constant, ~0.1 N/m. The cantilever's free oscillation amplitude A_0 and set-point amplitude A_s were set at 1−2 nm and ~0.9 × A_0, respectively. The imaging rate, scan size and the pixel size for each AFM image are 150 ms/frame, 60 × 60 nm^2 and 80 × 80 pixels, respectively.

Analysis of AFM Images

For analysis, AFM images were pretreated with a low-pass filter to remove spike noise and with a flatten filter to make the overall xy-plane flat, using a laboratory built software as described before (Ngo et al., 2015; Uchihashi et al., 2012). This software is available at https://elifesciences.org/content/4/e04806/article-data-fig-data-supplementary-material. The heights of molecules were measured semi-automatically using the following steps. First, the most probable highest point near the highest point of the molecule was selected manually. Second, the actual highest point was automatically determined by searching a 10 × 10 pixel area (typically 7.5 × 7.5 nm^2) around the selected point.

2D correlation coefficients were calculated between the HS-AFM images of the first frame and each of the frames within the Region of Interest (ROI) (i.e., the first frame is the reference) (Uchihashi et al., 2011). The sizes of the ROIs were about 25×25 nm^2. The 2D correlation coefficient was calculated frame-by-frame for each ROI. The 2D correlation coefficient r is defined as,

$$r = \frac{\sum_m \sum_n \left(H_{m\ \ n} - \overline{H}\right)\left(R_{m\ \ n} - \overline{R}\right)}{\sqrt{\left(\sum_m \sum_n \left(H_{m\ \ n} - \overline{H}\right)^2 \left(\sum_m \sum_n \left(R_{m\ \ n} - \overline{R}\right)^2}}$$

in which H_{mn} and R_{mn} are the heights at the pixel point (m, n) in the ROI to be analyzed and the reference ROI of the reference frame, respectively. $\overline{H}$ and $\overline{R}$ are the mean values of the height matrices H and R, respectively.

QUANTIFICATION AND STATISTICAL ANALYSIS

Statistics of the X-ray crystallographic and small angle-X-ray scattering data processing, refinement and structure validation are summarized in Table 1 and S1. ITC measurements were performed at least three times and the quantified data represent mean ± SD.

DATA AND SOFTWARE AVAILABILITY

The PDB accession number for apo-TTD is 5YYA and its complex with LIG1K126me3 peptide is 5YY9.